

Overlap reduction functions for pulsar timing arrays and astrometry

Keisuke Inomata,^{1,*} Marc Kamionkowski,^{1,†} Celia M. Toral,^{2,‡} and Stephen R. Taylor^{2,§}

¹*William H. Miller III Department of Physics & Astronomy,
Johns Hopkins University, 3400 N. Charles St., Baltimore, MD 21218, USA*

²*Department of Physics and Astronomy, Vanderbilt University,
2301 Vanderbilt Place, Nashville, Tennessee 37235, USA*

We present an efficient technique for calculating the angular two-point correlation functions (or “overlap reduction functions”) induced by gravitational waves in both the pulse arrival times of pulsars and in the angular deflections of distant sources. In the most general case, there are six auto- and cross-correlations for the pulse arrival times and the two components of the angular deflection. We provide results for spin-2 (i.e., general-relativistic) gravitational waves as well as the spin-1 modes that may arise in alternative-gravity theories. These calculations can be easily implemented for future analysis or study, and we provide code to do so.

I. INTRODUCTION

Evidence of a stochastic gravitational-wave background (SGWB) with periods of years to decades has recently been presented by four pulsar-timing array (PTAs) collaborations [1–4], broadening the landscape of observational gravitational wave (GW) science to encompass almost 11 orders of magnitude in frequency. These new observations call for increased efforts to characterize GWs at these \sim nHz frequencies. Some obvious next milestones beyond this first evidence include the search for anisotropy and polarization in the SGWB. Detection of either would provide additional information on the sources of these GWs which, at these frequencies, are expected to be from a population of binary supermassive black holes at mass scales of $\sim 10^8 - 10^{10} M_\odot$ [5–12], but may also arise from other, more exotic, sources [13–21].

The measurement process for PTAs relies on the apparent change to the spin period of pulsars induced by the passage of a GW between a pulsar and the Earth. The integrated effect over the path of photons from the pulsar to the Earth leads to a redshift to the pulse arrival rate, and (upon a further time integral) a deviation to the expected arrival time of radio pulses. By contrast, a SGWB at frequency ranges that overlap with the PTA sensitivity band may also be sought with astrometry [22–26]. The corresponding effect here is to induce deflections to measured positions of sources, such as stars or quasars. As such, one may consider PTAs and astrometry together to probe GWs through the 4-vector of light deflections. The key SGWB observable in astrometry is the angular two-point correlation function [24] of the positional deflections of widely separated sources, an analog of the Hellings-Downs curve [27] for pulsar time delays due to a Gaussian, stationary, isotropic, and unpolarized SGWB. Using astrometry, GAIA and extragalactic radio sources constrain the energy density of the SGWB to be $< 1.1\%$ of the Universe’s critical density for frequencies $6 \times 10^{-18} \text{ Hz} \lesssim f \lesssim 10^{-9} \text{ Hz}$ [28], which is quite a bit weaker than the values $\sim 10^{-8}$ implied by recent PTA results [e.g., 1]. However, there are prospects for future missions that might provide improved astrometric measurements [29, 30], and such measurements may also be possible with photometric surveys [31–33].

If the SGWB is isotropic and unpolarized—as most searches assume—then the two-point correlation functions depend only on the angle between the two points of measurement. If, however, the SGWB is anisotropic or polarized, then there may be more structure in the two-point correlation, analogous to that previously computed in a PTA context [34–45]. Indeed, the generalization of the astrometric angular two-point correlation function has already been performed for the case of a SGWB composed of non-Einsteinian GW polarizations [46, 47], which echoes analogous work for pulsar timing [25, 43, 45, 48–50]. Here, we present the first calculation of angular two-point correlations induced in astrometric deflections by anisotropies and linear or circular polarization in the SGWB. We generalize here the approach for timing residuals of Ref. [43] to the present case of angular deflections. This allows for fairly compact expressions for the correlation functions that are easily evaluated numerically. Results are presented for the spin-2 (tensor) GW polarizations that arise in general relativity, as well as the spin-1 (vector) polarizations that may arise in alternative-gravity theories [51, 52]. Similar to the previous work [43], we will not study the case of spin-0 (scalar) GWs, decomposed into scalar-transverse (ST) and scalar-longitudinal (SL) modes, for the following reasons. For ST modes, the redshift response and the deflection angle consist only of the monopole and the dipole moments [25], which

* inomata@jhu.edu

† kamion@jhu.edu

‡ celia.m.toral@Vanderbilt.Edu

§ stephen.r.taylor@Vanderbilt.Edu

limits the information of anisotropies of GW background that we can extract from the observations. For SL modes, we need a more careful treatment than for the spin-2 or spin-1 cases because the redshift response depends on the pulsar term [25, 53], whose analysis is beyond the scope of this paper.

We summarize here for the busy reader the key equations and relationships that can be used right away. First, we note that the deviation to a pulse arrival time is a scalar function on the sphere, while the angular deflection of a point's measured position is a vector on the two-dimensional celestial sphere. There are, therefore, most generally 6 possible auto- and cross-correlations for the combined data set from a PTA and an astrometry survey, all of which we derive. We also present details of the derivations, and as a result, the paper is long. Still, the central results are fairly compact. The most general PTA overlap reduction functions (ORFs), reprised from Ref. [43], can be obtained from Eq. (20) with coefficients $F_{\ell\ell'}^L$ given in Table I (for intensity anisotropy and circular and linear polarizations for spin-2 and spin-1 GWs). The ORFs for angular deflections are given in Eq. (52) with coefficients listed in Tables II-IV, which are derived here for the first time. For the cross-correlations between the PTA and the astrometry signals (also derived here for the first time), the ORFs are given in Eqs. (80) and (81) with the coefficients given in Eq. (84).

This paper is laid out as follows. In the following Section, we describe the characterization of the SGWB in terms of spherical-harmonic expansion coefficients for the intensity and circular- and linear-polarization patterns. Section III then calculates the ORFs, starting first with PTA timing residuals and then moving on to astrometry observables, and in each case, beginning with the spin-2 calculations and then following up with the spin-1 calculations. We make closing remarks in Section IV, and an Appendix provides some relevant properties of Wigner D matrices. We note that the code for the numerical calculation of the ORFs is available at [our Github page](#).

II. CHARACTERIZATION OF THE GRAVITATIONAL-WAVE BACKGROUND

In this work, we consider both spin-2 (tensor) and spin-1 (vector) GWs. We take the same characterization for the spin-2 GWs as Ref. [40] and generalize it to the spin-1 GWs with the convention in Ref. [54]. We expand the tensor fluctuation as

$$h_{ij}(t, x) = \int df \int d^2\hat{\Omega} \left[\sum_{\lambda=+, \times, x, y} \tilde{h}_\lambda(f, \hat{\Omega}) e_{ij}^\lambda(\hat{\Omega}) \right] e^{-2\pi i f(t - \hat{\Omega} \cdot x)}, \quad (1)$$

where $\hat{\Omega}$ is the unit vector for the propagation direction of the GWs. The explicit forms of the polarization tensors are given by

$$e_{ij}^+(\hat{\Omega}) = \hat{p}_i \hat{p}_j - \hat{q}_i \hat{q}_j, \quad e_{ij}^\times(\hat{\Omega}) = \hat{p}_i \hat{q}_j + \hat{q}_i \hat{p}_j, \quad (2)$$

$$e_{ij}^x(\hat{\Omega}) = \hat{\Omega}_i \hat{p}_j + \hat{\Omega}_j \hat{p}_i, \quad e_{ij}^y(\hat{\Omega}) = \hat{\Omega}_i \hat{q}_j + \hat{\Omega}_j \hat{q}_i, \quad (3)$$

where \hat{p} and \hat{q} are the unit vectors perpendicular to $\hat{\Omega}$ and they satisfy $\hat{p} \cdot \hat{q} = 0$. The polarizations in the first (second) line are for the spin-2 (spin-1) GWs. If we set \hat{p} , \hat{q} , and $\hat{\Omega}$ to be aligned with the x , y , and z axes respectively, the nonzero components of each polarization vector are $\epsilon_{xx}^+ = -\epsilon_{yy}^+ = 1$, $\epsilon_{xy}^\times = \epsilon_{yx}^\times = 1$, $\epsilon_{xz}^x = \epsilon_{zx}^x = 1$, and $\epsilon_{yz}^y = \epsilon_{zy}^y = 1$. Note that we take the normalization that gives $\epsilon^{\lambda ij} \epsilon_{ij}^{\lambda'} = 2\delta^{\lambda\lambda'}$. We hereafter assume that the spin-2 and the spin-1 GWs are uncorrelated. We formulate the anisotropies of the spin-2 and the spin-1 GWs, respectively, through

$$\left\langle \tilde{h}_{\lambda^t}^*(f, \hat{\Omega}) \tilde{h}_{\lambda^{t'}}(f', \hat{\Omega}') \right\rangle = \delta_D(f - f') \delta_D(\hat{\Omega}, \hat{\Omega}') \mathcal{P}_{\lambda^t \lambda^{t'}}^t(f, \hat{\Omega}), \quad (4)$$

$$\left\langle \tilde{h}_{\lambda^v}^*(f, \hat{\Omega}) \tilde{h}_{\lambda^{v'}}(f', \hat{\Omega}') \right\rangle = \delta_D(f - f') \delta_D(\hat{\Omega}, \hat{\Omega}') \mathcal{P}_{\lambda^v \lambda^{v'}}^v(f, \hat{\Omega}), \quad (5)$$

where $\lambda^t \in \{+, \times\}$ and $\lambda^v \in \{x, y\}$, δ_D is the delta function, and $\mathcal{P}_{\lambda\lambda'}$ is the spectral density of the GW background, which depends on the frequency, the polarization, and the propagation direction of GWs. We parametrize the spectral density as

$$\mathcal{P}_{\lambda\lambda'}^p = \begin{pmatrix} I^p(f, \hat{\Omega}) + Q^p(f, \hat{\Omega}) & U^p(f, \hat{\Omega}) - iV^p(f, \hat{\Omega}) \\ U^p(f, \hat{\Omega}) + iV^p(f, \hat{\Omega}) & I^p(f, \hat{\Omega}) - Q^p(f, \hat{\Omega}) \end{pmatrix}, \quad (6)$$

where $p \in \{t, v\}$. Specifically, we obtain

$$\begin{aligned} I^t(f, \hat{\Omega}) &= \frac{1}{2} \langle |\tilde{h}_+|^2 + |\tilde{h}_\times|^2 \rangle = \frac{1}{2} \langle |\tilde{h}_L^t|^2 + |\tilde{h}_R^t|^2 \rangle, & Q^t(f, \hat{\Omega}) &= \frac{1}{2} \langle |\tilde{h}_+|^2 - |\tilde{h}_\times|^2 \rangle, \\ U^t(f, \hat{\Omega}) &= \frac{1}{2} \langle \tilde{h}_+^* \tilde{h}_\times + \tilde{h}_\times^* \tilde{h}_+ \rangle, & V^t(f, \hat{\Omega}) &= \frac{1}{2i} \langle \tilde{h}_+^* \tilde{h}_\times - \tilde{h}_\times^* \tilde{h}_+ \rangle = \frac{1}{2} \langle |\tilde{h}_L^t|^2 - |\tilde{h}_R^t|^2 \rangle, \end{aligned} \quad (7)$$

$$\begin{aligned} I^v(f, \hat{\Omega}) &= \frac{1}{2} \langle |\tilde{h}_x|^2 + |\tilde{h}_y|^2 \rangle = \frac{1}{2} \langle |\tilde{h}_L^v|^2 + |\tilde{h}_R^v|^2 \rangle, & Q^v(f, \hat{\Omega}) &= \frac{1}{2} \langle |\tilde{h}_x|^2 - |\tilde{h}_y|^2 \rangle, \\ U^v(f, \hat{\Omega}) &= \frac{1}{2} \langle \tilde{h}_x^* \tilde{h}_y + \tilde{h}_y^* \tilde{h}_x \rangle, & V^v(f, \hat{\Omega}) &= \frac{1}{2i} \langle \tilde{h}_x^* \tilde{h}_y - \tilde{h}_y^* \tilde{h}_x \rangle = \frac{1}{2} \langle |\tilde{h}_L^v|^2 - |\tilde{h}_R^v|^2 \rangle, \end{aligned} \quad (8)$$

where the arguments of \tilde{h} have been omitted and the left-handed and the right-handed modes are defined as $\tilde{h}_L^t = (\tilde{h}_+ - i\tilde{h}_\times)/\sqrt{2}$, $\tilde{h}_R^t = (\tilde{h}_+ + i\tilde{h}_\times)/\sqrt{2}$, $\tilde{h}_L^v = (\tilde{h}_x - i\tilde{h}_y)/\sqrt{2}$, and $\tilde{h}_R^v = (\tilde{h}_x + i\tilde{h}_y)/\sqrt{2}$. For convenience, we define P^\pm as

$$P^{t,\pm}(f, \hat{\Omega}) \equiv Q^t \pm iU^t = \frac{1}{2} \langle (\tilde{h}_+ \mp i\tilde{h}_\times)^* (\tilde{h}_+ \pm i\tilde{h}_\times) \rangle, \quad (9)$$

$$P^{v,\pm}(f, \hat{\Omega}) \equiv Q^v \pm iU^v = \frac{1}{2} \langle (\tilde{h}_x \mp i\tilde{h}_y)^* (\tilde{h}_x \pm i\tilde{h}_y) \rangle, \quad (10)$$

and can rewrite this as

$$P^{p,+}(f, \hat{\Omega}) = \langle \tilde{h}_L^{p*} \tilde{h}_R^p \rangle, \quad P^{p,-}(f, \hat{\Omega}) = \langle \tilde{h}_R^{p*} \tilde{h}_L^p \rangle. \quad (11)$$

These Stokes parameters are expanded as

$$I^p(f, \hat{\Omega}) = I_0^p(f) \sum_{L=0}^{\infty} \sum_{M=-L}^L c_{LM}^{p,I}(f) Y_{LM}(\hat{\Omega}), \quad (12)$$

$$V^p(f, \hat{\Omega}) = I_0^p(f) \sum_{L=0}^{\infty} \sum_{M=-L}^L c_{LM}^{p,V}(f) Y_{LM}(\hat{\Omega}), \quad (13)$$

$$P^{t,\pm}(f, \hat{\Omega}) = I_0^t(f) \sum_{L=4}^{\infty} \sum_{M=-L}^L c_{LM}^{t,\pm}(f) {}_{\pm 4}Y_{LM}(\hat{\Omega}), \quad (14)$$

$$P^{v,\pm}(f, \hat{\Omega}) = I_0^v(f) \sum_{L=2}^{\infty} \sum_{M=-L}^L c_{LM}^{v,\pm}(f) {}_{\pm 2}Y_{LM}(\hat{\Omega}), \quad (15)$$

where we normalize $I_0^p(f)$ such that $c_{00}^{p,I}(f) = 1$. For later convenience, we here introduce the spherical-harmonic coefficients for the scalar E and pseudo-scalar B modes in the linear polarization map (P^\pm), analogous to the CMB polarizations:

$$c_{LM}^{p,E} = \frac{1}{2} (c_{LM}^{p,+} + c_{LM}^{p,-}), \quad c_{LM}^{p,B} = \frac{1}{2i} (c_{LM}^{p,+} - c_{LM}^{p,-}). \quad (16)$$

III. OVERLAP REDUCTION FUNCTIONS

We consider two quantities. One is the redshift response z of PTA observation for GWs, and the other is a deflection-angle field $\delta\vec{n}$ in astrometry probes. We will obtain the exact formulas for all the ORFs associated with PTA and astrometry, while showing the numerical results for some of them. We refer to [our Github page](#) for the numerical results of all the ORFs.

A. Auto-correlation of redshift responses

We first consider the auto-correlation of the redshift responses in PTA observations. The redshift response is related to the GWs propagating along $\hat{\Omega}$ as [55]

$$z(t|\hat{\Omega}) = \frac{\hat{n}_a^i \hat{n}_a^j \Delta h_{ij}(t, \hat{\Omega})}{2(1 + \hat{\Omega} \cdot \hat{n}_a)}, \quad (17)$$

where the subscript a labels a given pulsar and $L_a \hat{n}_a$ is the position of the pulsar from solar system barycenter, located at $\bar{0}$. We here define $\Delta h_{ij} \equiv h_{ij}(t, \hat{\Omega}, \bar{0}) - h_{ij}(t_p, \hat{\Omega}, L_a \hat{n}_a)$ as the difference of the tensor fluctuations between the solar barycenter at t and the pulsar at $t_p = t - L_a$. However, similar to existing analysis, such as Ref. [43], we disregard the contributions of the tensor fluctuations at the pulsar throughout this work.

Although the ORF for this case was studied in Ref. [43], we summarize the calculation for completeness. Throughout this work, we focus on the contribution from a single frequency bin f . Then, we can expand z as

$$z_f(\hat{n}) = \sum_{\ell m} Y_{\ell m}(\theta, \phi) z_{f, \ell m}. \quad (18)$$

Note that z_f is a Fourier mode and can be complex.

We consider the two-point correlation function:

$$\begin{aligned} \langle z_f^*(\hat{n}_a) z_f(\hat{n}_b) \rangle &= \sum_{\ell m} \sum_{\ell' m'} \langle z_{f, \ell m}^* z_{f, \ell' m'} \rangle Y_{\ell m}^*(\hat{n}_a) Y_{\ell' m'}(\hat{n}_b) \\ &= \sum_{p=t, v} \sum_X i^X \left[I_0^p \sum_{L, M} c_{LM}^{p, X} \Gamma_{LM}^{p, X, zz}(\hat{n}_a, \hat{n}_b) \right], \end{aligned} \quad (19)$$

where the average is over the ensemble of realizations of the GW background, and $X \in \{I, V, E, B\}$ and $i^X = i$ for $X = B$ and $i^X = 1$ for the others throughout this work.¹ Here, Γ_{LM} is the ORF, given by

$$\Gamma_{LM}^{p, X, zz}(\hat{n}_a, \hat{n}_b) = (-1)^L \sqrt{\pi} \sum_{\ell=\ell_{\min}}^{\ell_{\max}} \sum_{\ell'=\ell_{\min}}^{\ell_{\max}} F_{\ell \ell'}^{L, p, X, zz} \{Y_{\ell}(\hat{n}_a) \otimes Y_{\ell'}(\hat{n}_b)\}_{LM}, \quad (20)$$

where

$$\{Y_{\ell}(\hat{n}_a) \otimes Y_{\ell'}(\hat{n}_b)\}_{LM} = \sum_{m=-\ell}^{\ell} \sum_{m'=-\ell'}^{\ell'} \langle \ell m \ell' m' | LM \rangle Y_{\ell m}(\hat{n}_a) Y_{\ell' m'}(\hat{n}_b) \quad (21)$$

is a bipolar spherical harmonic (BiPoSH) [56–59] and we have explicitly shown the lower and the upper bounds for the sums. We will see that $\ell_{\min} = 2$ for the spin-2 GWs and $\ell_{\min} = 1$ for the spin-1 GWs below Eqs. (24) and (37). Strictly speaking, $\ell_{\max} = \infty$. However, the numerical calculation of the ORFs with $\ell_{\max} = \infty$ requires an infinite computational cost. Fortunately, if we set ℓ_{\max} to be large enough, the obtained ORFs become insensitive to a concrete value of ℓ_{\max} . In this work, for the numerical calculation, we change the value of ℓ_{\max} depending on the ORFs. In particular, we take larger ℓ_{\max} for the ORFs including redshift response due to spin-1 GWs because they slowly converge compared to the other quantities, as we will see below. We also note that the E- and the B-mode ORFs (Γ_{LM}^E and Γ_{LM}^B) are zero for $L < 4$ for spin-2 GWs and for $L < 2$ for spin-1 GWs because of the properties of the spin-weighted spherical harmonics, ${}_s Y_{\ell m} = 0$ for $\ell < |s|$ (see the lower bounds of L in Eqs. (14) and (15)). All the nontrivial information about the ORFs is included in the expressions of $F_{\ell \ell'}^{L, p, X, zz}$, which we will obtain in the following.

1. Spin-2 GWs

We here consider the spin-2 GWs, described by the $+$ and \times modes. From Eq. (17), the redshift response due to the tensor perturbations with the frequency f and the propagation direction \hat{k} becomes

$$\begin{aligned} z_f(\hat{n}|\hat{k}) &= \frac{1}{2} \left[\tilde{h}^+(f, \hat{k})(1 - \cos \theta) \cos(2\phi) + \tilde{h}^\times(f, \hat{k})(1 - \cos \theta) \sin(2\phi) \right] \\ &= \frac{1}{2\sqrt{2}} \left[\tilde{h}_L^t(f, \hat{k})(1 - \cos \theta) e^{2i\phi} + \tilde{h}_R^t(f, \hat{k})(1 - \cos \theta) e^{-2i\phi} \right], \end{aligned} \quad (22)$$

¹ Note that the convention for i^X for V differs from that in Ref. [43].

where we have taken the coordinates of $\hat{k} = (0, 0, 1)$ and $\hat{n} = (\sin \theta \cos \phi, \sin \theta \sin \phi, \cos \theta)$. From this, we can obtain

$$\begin{aligned}\tilde{z}_{f,\ell m}(\hat{k}) &= \int d^2 \hat{n} Y_{\ell m}^*(\hat{n}) z_f(\hat{n}|\hat{k}) \\ &= \frac{z_\ell^t}{\sqrt{2}} \left(\tilde{h}_L^t(f, \hat{k}) \delta_{m2} + \tilde{h}_R^t(f, \hat{k}) \delta_{m,-2} \right),\end{aligned}\quad (23)$$

where

$$z_\ell^t \equiv (-1)^\ell \sqrt{\frac{4\pi(2\ell+1)(\ell-2)!}{(\ell+2)!}}. \quad (24)$$

We can find $z_{f,\ell m} = 0$ in $\ell < 2$ because $Y_{\ell m} = 0$ for $\ell < |m|$, which leads to $\ell_{\min} = 2$ in Eq. (20) for the spin-2 GWs. Then, we move to the general case with a propagation direction $\hat{\Omega}$. To this end, we use the following relation with Wigner D -matrix, $D_{mm'}^{(\ell)}$ [60]:

$$z_f(\hat{n}|\hat{\Omega}) = \sum_{\ell} \sum_{mm'} Y_{\ell m}(\hat{\Omega}) D_{mm'}^{(\ell)}(\hat{\Omega}) \tilde{z}_{f,\ell m'}(\hat{k}), \quad (25)$$

where $D_{mm'}^{(\ell)}(\hat{\Omega}) = D_{mm'}^{(\ell)}(\phi, \theta, 0)$ with $\hat{\Omega} = (\theta, \phi)$. See also Appendix A for the properties of Wigner D -matrix. From this, we obtain

$$\begin{aligned}\tilde{z}_{f,\ell m}(\hat{\Omega}) &= \int d\hat{n} Y_{\ell m}^*(\hat{n}) z_f(\hat{n}|\hat{\Omega}) \\ &= \frac{z_\ell^t}{\sqrt{2}} \left(\tilde{h}_L^t(f, \hat{\Omega}) D_{m,2}^{(\ell)} + \tilde{h}_R^t(f, \hat{\Omega}) D_{m,-2}^{(\ell)} \right).\end{aligned}\quad (26)$$

We here define $z_{f,\ell m} = \int d^2 \hat{\Omega} \tilde{z}_{f,\ell m}(\hat{\Omega})$ and obtain

$$\begin{aligned}\langle z_{f,\ell m}^* z_{f,\ell' m'} \rangle &= \frac{z_\ell^t z_{\ell'}^t}{2} \int d^2 \hat{\Omega} \int d^2 \hat{\Omega}' \left\langle \left[\tilde{h}_L^{t,*}(f, \hat{\Omega}) D_{m,2}^{(\ell)*} + \tilde{h}_R^{t,*}(f, \hat{\Omega}) D_{m,-2}^{(\ell)*} \right] \left[\tilde{h}_L^t(f, \hat{\Omega}') D_{m,2}^{(\ell)} + \tilde{h}_R^t(f, \hat{\Omega}') D_{m,-2}^{(\ell)} \right] \right\rangle \\ &= \frac{z_\ell^t z_{\ell'}^t}{2} \int_0^t \sum_{LM} \left[c_{LM}^{t,I} \left({}^{(0,2,2)} W_{\ell\ell'mm'}^{LM} + {}^{(0,-2,-2)} W_{\ell\ell'mm'}^{LM} \right) + c_{LM}^{t,V} \left({}^{(0,2,2)} W_{\ell\ell'mm'}^{LM} - {}^{(0,-2,-2)} W_{\ell\ell'mm'}^{LM} \right) \right. \\ &\quad \left. + c_{LM}^{t,+} {}^{(4,2,-2)} W_{\ell\ell'mm'}^{LM} + c_{LM}^{t,-} {}^{(-4,-2,2)} W_{\ell\ell'mm'}^{LM} \right].\end{aligned}\quad (27)$$

${}^{(abc)} W_{\ell\ell'mm'}^{LM}$ is defined as

$$\begin{aligned}{}^{(abc)} W_{\ell\ell'mm'}^{LM} &\equiv \int d^2 \hat{\Omega} {}_a Y_{LM}(\hat{\Omega}) D_{mb}^{(\ell)*}(\hat{\Omega}) D_{m'c}^{(\ell')}(\hat{\Omega}) \\ &= (-1)^{b+m'} \frac{4\pi}{\sqrt{(2\ell+1)(2\ell'+1)}} \int d^2 \hat{\Omega} {}_a Y_{LM}(\hat{\Omega}) {}_{-b} Y_{\ell m}(\hat{\Omega}) {}_c Y_{\ell' -m'}(\hat{\Omega}) \\ &= (-1)^{b+m'} \sqrt{4\pi(2L+1)} \begin{pmatrix} L & \ell & \ell' \\ M & m & -m' \end{pmatrix} \begin{pmatrix} L & \ell & \ell' \\ -a & b & -c \end{pmatrix} \\ &= 2(-1)^{2\ell+M+L+b+m'} \sqrt{\pi} \langle \ell(-m)\ell'm' | LM \rangle \begin{pmatrix} L & \ell & \ell' \\ -a & b & -c \end{pmatrix},\end{aligned}\quad (28)$$

where we have used the following relation between Wigner D -matrix and spin-weighted spherical harmonics [50],

$$D_{m'm}^\ell(\phi, \theta, \psi) = (-1)^{m'} \sqrt{\frac{4\pi}{2\ell+1}} {}_m Y_{\ell, -m'}(\theta, \phi) e^{-im\psi}, \quad (29)$$

$$[D_{m'm}^\ell(\phi, \theta, \psi)]^* = (-1)^m \sqrt{\frac{4\pi}{2\ell+1}} {}_{-m} Y_{\ell, m'}(\theta, \phi) e^{im\psi}, \quad (30)$$

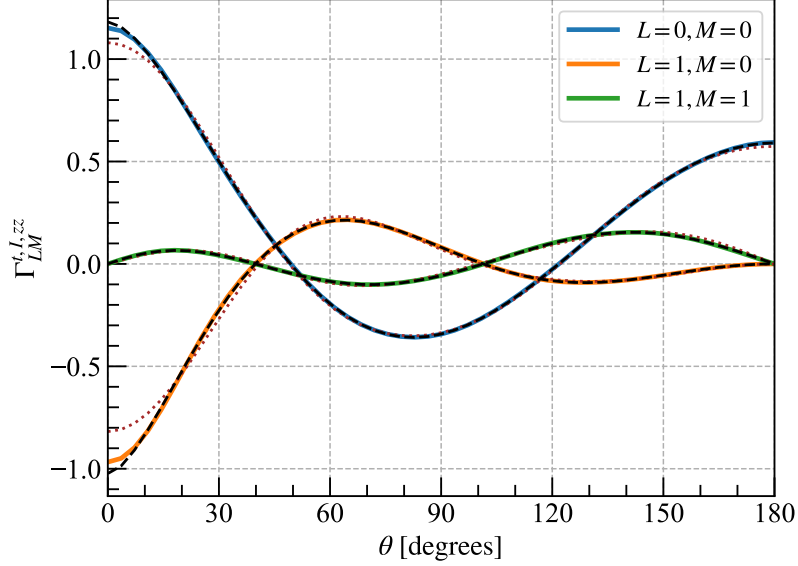


FIG. 1. The ORFs of $\Gamma_{LM}^{t,I,zz}(\theta)$ in the coordinates of Eq. (34). The color solid lines are for $\ell_{\max} = 10$. The brown dotted lines are for $\ell_{\max} = 5$. The black dashed lines are the exact analytical results obtained in Ref. [35].

and the integral of the product of three spherical harmonics [50, 60]²

$$\begin{aligned} & \int d^2\hat{\Omega} \, s_1 Y_{\ell_1 m_1}(\hat{\Omega}) \, s_2 Y_{\ell_2 m_2}(\hat{\Omega}) \, s_3 Y_{\ell_3 m_3}(\hat{\Omega}) \\ &= \sqrt{\frac{(2\ell_1+1)(2\ell_2+1)(2\ell_3+1)}{4\pi}} \begin{pmatrix} \ell_1 & \ell_2 & \ell_3 \\ m_1 & m_2 & m_3 \end{pmatrix} \begin{pmatrix} \ell_1 & \ell_2 & \ell_3 \\ -s_1 & -s_2 & -s_3 \end{pmatrix}. \end{aligned} \quad (31)$$

Also, Wigner 3-j symbols are related to the Clebsch-Gordan coefficients as

$$\begin{aligned} \begin{pmatrix} L & \ell_1 & \ell_2 \\ M & m_1 & m_2 \end{pmatrix} &= \frac{(-1)^{\ell_1-\ell_2+M}}{\sqrt{2L+1}} \langle \ell_1 m_1 \ell_2 m_2 | L(-M) \rangle \\ &= \frac{(-1)^{2\ell_1+M+L}}{\sqrt{2L+1}} \langle \ell_1(-m_1) \ell_2(-m_2) | LM \rangle. \end{aligned} \quad (32)$$

Then, we can rewrite Eq. (27) as

$$\begin{aligned} \langle z_{f,\ell m}^* z_{f,\ell' m'} \rangle &= 2z_\ell^t z_{\ell'}^t I_0^t \sum_{LM} (-1)^{m+L} \sqrt{\pi} \langle \ell(-m) \ell' m' | LM \rangle \\ &\times \left\{ \left[c_{LM}^{t,I} X_{\ell\ell'}^L - c_{LM}^{t,V} (1 - X_{\ell\ell'}^L) \right] \begin{pmatrix} \ell & \ell' & L \\ -2 & 2 & 0 \end{pmatrix} + \left[c_{LM}^{t,E} X_{\ell\ell'}^L + i c_{LM}^{t,B} (1 - X_{\ell\ell'}^L) \right] \begin{pmatrix} \ell & \ell' & L \\ 2 & 2 & -4 \end{pmatrix} \right\}, \end{aligned} \quad (33)$$

where $X_{\ell\ell'}^L = 1$ for $\ell + \ell' + L = \text{even}$ and 0 otherwise. Substituting this into Eq. (19), we finally obtain the coefficients $F_{\ell\ell'}^L$ in Eq. (20), summarized in the left column of Table I.

To get the concrete plots of the ORF, we take the following coordinate choice throughout this work:

$$\hat{n}_a = (0, 0, 1), \quad \hat{n}_b = (\sin \theta, 0, \cos \theta). \quad (34)$$

In these coordinates, the ORF only depends on θ . Figure 1 shows the θ dependence of $\Gamma_{LM}^{t,I,zz}$ with different ℓ_{\max} , where we also show the exact analytical results in Ref. [35]. From this figure, we can see that $\ell_{\max} = 10$ is a good value for the convergence for spin-2 GW case.

² The integral of the product of three Wigner D -matrices is explicitly shown in Ref. [60], from which we can obtain Eq. (31).

X	Spin-2	Spin-1
I	$2z_\ell^t z_{\ell'}^t \begin{pmatrix} \ell & \ell' & L \\ -2 & 2 & 0 \end{pmatrix} X_{\ell\ell'}^L$	$-2z_\ell^v z_{\ell'}^v \begin{pmatrix} \ell & \ell' & L \\ -1 & 1 & 0 \end{pmatrix} X_{\ell\ell'}^L$
V	$-2z_\ell^t z_{\ell'}^t \begin{pmatrix} \ell & \ell' & L \\ -2 & 2 & 0 \end{pmatrix} (1 - X_{\ell\ell'}^L)$	$2z_\ell^v z_{\ell'}^v \begin{pmatrix} \ell & \ell' & L \\ -1 & 1 & 0 \end{pmatrix} (1 - X_{\ell\ell'}^L)$
E	$2z_\ell^t z_{\ell'}^t \begin{pmatrix} \ell & \ell' & L \\ 2 & 2 & -4 \end{pmatrix} X_{\ell\ell'}^L$	$2z_\ell^v z_{\ell'}^v \begin{pmatrix} \ell & \ell' & L \\ 1 & 1 & -2 \end{pmatrix} X_{\ell\ell'}^L$
B	$2z_\ell^t z_{\ell'}^t \begin{pmatrix} \ell & \ell' & L \\ 2 & 2 & -4 \end{pmatrix} (1 - X_{\ell\ell'}^L)$	$2z_\ell^v z_{\ell'}^v \begin{pmatrix} \ell & \ell' & L \\ 1 & 1 & -2 \end{pmatrix} (1 - X_{\ell\ell'}^L)$

TABLE I. The expressions of $F_{\ell\ell'}^{L,p,X,zz}$ that appear in Eq. (20) for the ORFs for intensity (I), circular-polarization (V), and E- and B-mode linear-polarization anisotropies of multipole L . See Eq. (24) for z_ℓ^t and Eq. (37) for z_ℓ^v .

2. Spin-1 GWs

Next, we consider the spin-1 GWs. The procedure is basically the same as the case of spin-2 GWs. From Eq. (17), the redshift response due to the spin-1 GWs with the frequency f and the propagation direction \hat{k} becomes

$$\begin{aligned} z(\hat{n}|\hat{k}) &= \frac{1}{2} \left[\tilde{h}^x \frac{\sin 2\theta \cos \phi}{1 + \cos \theta} + \tilde{h}^y \frac{\sin 2\theta \sin \phi}{1 + \cos \theta} \right] \\ &= \frac{1}{2\sqrt{2}} \left[\tilde{h}_L^v \frac{\sin 2\theta}{1 + \cos \theta} e^{i\phi} + \tilde{h}_R^v \frac{\sin 2\theta}{1 + \cos \theta} e^{-i\phi} \right]. \end{aligned} \quad (35)$$

From this, we can obtain

$$\begin{aligned} \tilde{z}_{f,\ell m}(\hat{k}) &= \int d^2\hat{n} Y_{\ell m}^*(\hat{n}) z_f(\hat{n}|\hat{k}) \\ &= \frac{z_\ell^v}{\sqrt{2}} \left(\tilde{h}_L^v(f, \hat{k}) \delta_{m1} - \tilde{h}_R^v(f, \hat{k}) \delta_{m,-1} \right), \end{aligned} \quad (36)$$

where

$$z_\ell^v \equiv (-1)^{\ell+1} \sqrt{4\pi(2\ell+1)} \left(\frac{1}{\sqrt{\ell(\ell+1)}} - \frac{\sqrt{2}}{3} \delta_{\ell 1} \right). \quad (37)$$

Similar to the spin-2 GW case, we can find $z_{f,\ell m} = 0$ in $\ell < 1$, which leads to $\ell_{\min} = 1$ in Eq. (20) for the spin-1 GWs. We here generalize this to the case of GWs propagating in $\hat{\Omega}$:

$$\begin{aligned} \tilde{z}_{f,\ell m}(\hat{\Omega}) &= \int d\hat{n} Y_{\ell m}^*(\hat{n}) z_f(\hat{n}|\hat{\Omega}) \\ &= \frac{z_\ell^v}{\sqrt{2}} \left(\tilde{h}_L^v(f, \hat{\Omega}) D_{m',1}^{(\ell')} - \tilde{h}_R^v(f, \hat{\Omega}) D_{m',-1}^{(\ell')} \right). \end{aligned} \quad (38)$$

Using this, we finally obtain

$$\begin{aligned} \langle z_{f,\ell m}^* z_{f,\ell' m'} \rangle &= \frac{z_\ell^v z_{\ell'}^v}{2} \int d^2\hat{\Omega} \int d^2\hat{\Omega}' \left[\tilde{h}_L^{v,*}(f, \hat{\Omega}) D_{m,1}^{(\ell)*} - \tilde{h}_R^{v,*}(f, \hat{\Omega}) D_{m,-1}^{(\ell)*} \right] \left[\tilde{h}_L^v(f, \hat{\Omega}') D_{m',1}^{(\ell')} - \tilde{h}_R^v(f, \hat{\Omega}') D_{m',-1}^{(\ell')} \right] \\ &= \frac{z_\ell^v z_{\ell'}^v}{2} I_0^v \sum_{LM} \left[c_{LM}^v \left({}^{(0,1,1)}W_{\ell\ell'mm'}^{LM} + {}^{(0,-1,-1)}W_{\ell\ell'mm'}^{LM} \right) + c_{LM}^{v,V} \left({}^{(0,1,1)}W_{\ell\ell'mm'}^{LM} - {}^{(0,-1,-1)}W_{\ell\ell'mm'}^{LM} \right) \right] \end{aligned}$$

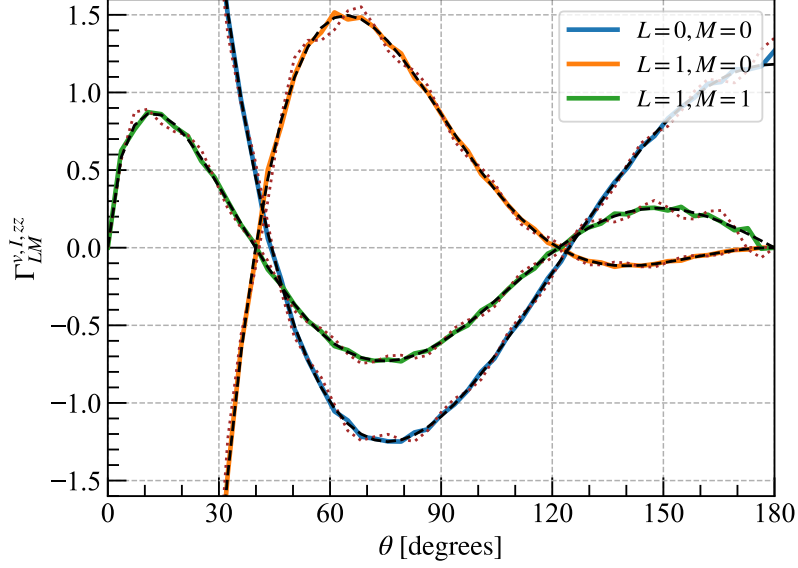


FIG. 2. The ORFs of $\Gamma_{LM}^{v,I,zz}(\theta)$. The color solid lines are for $\ell_{\max} = 40$. The brown dotted lines are for $\ell_{\max} = 20$. The black dashed lines are the exact analytical results obtained in Ref. [50]. Note that the $M = 0$ cases diverge at $\theta = 0$ [50].

$$\begin{aligned}
& \left[-c_{LM}^{v,+ (2,1,-1)} W_{\ell\ell'mm'}^{LM} - c_{LM}^{v,- (-2,-1,1)} W_{\ell\ell'mm'}^{LM} \right] \\
& = 2z_\ell^v z_{\ell'}^v I_0^v \sum_{LM} (-1)^{m+L} \sqrt{\pi} \langle \ell(-m)\ell'm' | LM \rangle \\
& \quad \times \left\{ \left[-c_{LM}^{v,I} X_{\ell\ell'}^L + c_{LM}^{v,V} (1 - X_{\ell\ell'}^L) \right] \begin{pmatrix} \ell & \ell' & L \\ -1 & 1 & 0 \end{pmatrix} + \left[c_{LM}^{v,E} X_{\ell\ell'}^L + i c_{LM}^{v,B} (1 - X_{\ell\ell'}^L) \right] \begin{pmatrix} \ell & \ell' & L \\ 1 & 1 & -2 \end{pmatrix} \right\}, \quad (39)
\end{aligned}$$

Substituting this into Eq. (19), we obtain the coefficient $F_{\ell\ell'}^L$, summarized in the right column of Table I. Figure 2 shows $\Gamma_{LM}^{v,I,zz}(\theta)$ with different ℓ_{\max} in the coordinates of Eq. (34). In the figure, We also show the exact analytical results in Ref. [35]. The convergence with respect to ℓ_{\max} is slower than the spin-2 GW case (Fig. 1). This is because z_ℓ^v decays slower than z_ℓ^t in $\ell \gg 1$ ($z_\ell^v \propto \ell^{-1/2}$ and $z_\ell^t \propto \ell^{-3/2}$ in $\ell \gg 1$).

B. Auto-correlation of deflection fields

Next, we consider the angular deflection due to GWs, expressed as $\hat{n}_{\text{obs}} = \hat{n} + \delta\vec{n}(\hat{n})$ with \hat{n}_{obs} being the observed celestial angle for stars or quasars and \hat{n} being that in the case without GWs. The angular deflection field caused by GWs propagating in $\hat{\Omega}$ is given by [24]

$$\delta n^i(t|\hat{n}) = \frac{(\hat{n}^i + \hat{\Omega}^i)\hat{n}^j\hat{n}^k h_{jk}(t, \hat{\Omega}, \vec{0})}{2(1 + \hat{n} \cdot \hat{\Omega})} - \frac{1}{2}\hat{n}^j h_{ij}(t, \hat{\Omega}, \vec{0}), \quad (40)$$

where the origin $\vec{0}$ corresponds to the observer position. In the following, we raise or lower the spatial indices with the Kronecker delta, e.g. $\delta n^i = \delta^{ij}\delta n_j$. We expand the deflection vector $\delta\vec{n}$ as

$$\delta n_i(\hat{n}) = \sum_{\ell m} \left[E_{\ell m} Y_{(\ell m)_i}^E + B_{\ell m} Y_{(\ell m)_i}^B \right], \quad (41)$$

where we take the same notation of the vector spherical harmonics as Refs. [25, 61]:

$$\begin{aligned}
Y_{(\ell m)_i}^E(\theta, \phi) &= -\frac{r}{\sqrt{\ell(\ell+1)}} \nabla_i Y_{\ell m}(\theta, \phi) = -\frac{1}{\sqrt{\ell(\ell+1)}} \left[\hat{\theta}_i \frac{\partial}{\partial \theta} + \hat{\phi}_i \frac{1}{\sin \theta} \frac{\partial}{\partial \phi} \right] Y_{\ell m}(\theta, \phi) \\
&= -\frac{1}{2\sqrt{\ell(\ell+1)}} \left\{ \hat{\theta}_i \left[\sqrt{(\ell-m)(\ell+m+1)} e^{-i\phi} Y_{\ell, m+1}(\theta, \phi) - \sqrt{(\ell+m)(\ell-m+1)} e^{i\phi} Y_{\ell, m-1}(\theta, \phi) \right] \right. \\
&\quad \left. + \hat{\phi}_i \frac{2im}{\sin \theta} Y_{\ell m}(\theta, \phi) \right\}, \tag{42}
\end{aligned}$$

$$\begin{aligned}
Y_{(\ell m)_i}^B(\theta, \phi) &= -\frac{r}{\sqrt{\ell(\ell+1)}} \epsilon_{ijk} \hat{n}^j \nabla^k Y_{\ell m}(\theta, \phi) = -\frac{1}{\sqrt{\ell(\ell+1)}} \left[\hat{\phi}_i \frac{\partial}{\partial \theta} - \hat{\theta}_i \frac{1}{\sin \theta} \frac{\partial}{\partial \phi} \right] Y_{\ell m}(\theta, \phi) \\
&= -\frac{1}{2\sqrt{\ell(\ell+1)}} \left\{ \hat{\phi}_i \left[\sqrt{(\ell-m)(\ell+m+1)} e^{-i\phi} Y_{\ell, m+1}(\theta, \phi) - \sqrt{(\ell+m)(\ell-m+1)} e^{i\phi} Y_{\ell, m-1}(\theta, \phi) \right] \right. \\
&\quad \left. - \hat{\theta}_i \frac{2im}{\sin \theta} Y_{\ell m}(\theta, \phi) \right\}, \tag{43}
\end{aligned}$$

where r is the radial distance, which is cancelled by r^{-1} in ∇_i , and $\hat{\theta}$ and $\hat{\phi}$ are the unit vectors satisfying $\hat{\theta} \cdot \hat{n} = \hat{\phi} \cdot \hat{n} = 0$ and being along the θ and the ϕ variation, respectively. Note the above vector spherical harmonics live on the surface perpendicular to \hat{n} . We define the spatial indices as those satisfying $\hat{\theta}_\theta = \hat{\phi}_\phi = 1$ and $\hat{\theta}_\phi = \hat{\phi}_\theta = 0$. With the additional spatial derivative, we find the following relation satisfied:

$$r \nabla^i Y_{(\ell m)_i}^E = -\frac{r^2}{\sqrt{\ell(\ell+1)}} \nabla^2 Y_{\ell m}(\theta, \phi) = \sqrt{\ell(\ell+1)} Y_{\ell m}(\theta, \phi), \tag{44}$$

$$r(\epsilon_{ijk} \hat{n}^j \nabla^k) Y_{(\ell m)_i}^B = -\frac{r^2}{\sqrt{\ell(\ell+1)}} \nabla^2 Y_{\ell m}(\theta, \phi) = \sqrt{\ell(\ell+1)} Y_{\ell m}(\theta, \phi), \tag{45}$$

where we have used $r^2 \nabla^2 Y_{\ell m} = -\ell(\ell+1) Y_{\ell m}$. Using this, we define

$$\bar{E}(\hat{n}) \equiv r \nabla_i \delta n^i = \sum_{\ell m} \bar{E}_{\ell m} Y_{\ell m}, \tag{46}$$

$$\bar{B}(\hat{n}) \equiv r(\epsilon_{ijk} \hat{n}^j \nabla^k) \delta n^i = \sum_{\ell m} \bar{B}_{\ell m} Y_{\ell m}, \tag{47}$$

where

$$\bar{E}_{\ell m} \equiv \sqrt{\ell(\ell+1)} E_{\ell m}, \quad \bar{B}_{\ell m} \equiv \sqrt{\ell(\ell+1)} B_{\ell m}. \tag{48}$$

From Eq. (40), we can also define a scalar $\bar{E}(t|\hat{n})$ and pseudoscalar $\bar{B}(t|\hat{n})$ induced by GWs propagating in $\hat{\Omega}$ as

$$\bar{E}(t|\hat{n}) = -\frac{1}{2} \text{Tr} h(t, \hat{\Omega}, \vec{0}) + \frac{(\hat{n}^i + \hat{\Omega}^i) \hat{n}^j h_{ij}(t, \hat{\Omega}, \vec{0})}{1 + \hat{\Omega} \cdot \hat{n}}, \tag{49}$$

$$\bar{B}(t|\hat{n}) = \epsilon^{ijk} \frac{\hat{\Omega}_i \hat{n}^l \hat{n}_k h_{jl}(t, \hat{\Omega}, \vec{0})}{1 + \hat{\Omega} \cdot \hat{n}}, \tag{50}$$

where we have used $r \nabla_i \hat{n}_j = \delta_{ij} - \hat{n}_i \hat{n}_j$.

Similar to the redshift response case (Eq. (19)), we consider the two-point correlation function:

$$\begin{aligned}
\langle \delta n_{f,i}^*(\hat{n}_a) \delta n_{f,j}(\hat{n}_b) \rangle &= \sum_{\ell m} \sum_{\ell' m'} \sum_{S, T} \langle S_{f, \ell m}^* T_{f, \ell' m'} \rangle Y_{(\ell m)_i}^{S*}(\hat{n}_a) Y_{(\ell' m')_j}^T(\hat{n}_b) \\
&= \sum_{p=\ell, v} \sum_X \sum_{S, T} i^X \left[I_0^p \sum_{L, M} c_{LM}^{p, X} \Gamma_{LM, ij}^{p, X, ST}(\hat{n}_a, \hat{n}_b) \right], \tag{51}
\end{aligned}$$

where $S, T \in \{E, B\}$. We note that there are two types of E and B modes here: those for the polarization of GWs and those for the deflection angle. Then, the ORF is given by

$$\Gamma_{(LM)ij}^{p,X,ST}(\hat{n}_a, \hat{n}_b) = (-1)^L \sqrt{\pi} \sum_{\ell=\ell_{\min}}^{\ell_{\max}} \sum_{\ell'=\ell_{\min}}^{\ell_{\max}} F_{\ell\ell'}^{L,p,X,ST} \left\{ Y_{(\ell)i}^S(\hat{n}_a) \otimes Y_{(\ell')j}^T(\hat{n}_b) \right\}_{LM}, \quad (52)$$

where

$$\left\{ Y_{(\ell)i}^S(\hat{n}_a) \otimes Y_{(\ell')j}^T(\hat{n}_b) \right\}_{LM} \equiv \sum_{m=-\ell}^{\ell} \sum_{m'=-\ell'}^{\ell'} \langle \ell m \ell' m' | LM \rangle Y_{(\ell m)i}^S(\hat{n}_a) Y_{(\ell' m')j}^T(\hat{n}_b). \quad (53)$$

We will obtain the expression of $F_{\ell\ell'}^{L,p,X,ST}$ in the following.

1. Spin-2 GWs

We begin with spin-2 GWs. The main goal of this subsection is to calculate $\langle S_{f,\ell m}^* T_{f,\ell' m'} \rangle$ and obtain their ORF. For convenience, we first obtain $\bar{E}_{\ell m}$ and $\bar{B}_{\ell m}$ and then convert them to $E_{\ell m}$ and $B_{\ell m}$. From Eqs. (49) and (50), the E - and B -modes of the deflection due to the spin-2 GWs with the frequency f and the propagation direction \hat{k} become

$$\begin{aligned} \bar{E}_f(\hat{n}|\hat{k}) &= \tilde{h}_+(1 - \cos\theta) \cos(2\phi) + \tilde{h}_\times(1 - \cos\theta) \sin(2\phi) \\ &= \frac{1}{\sqrt{2}} \left[\tilde{h}_L^t(1 - \cos\theta) e^{2i\phi} + \tilde{h}_R^t(1 - \cos\theta) e^{-2i\phi} \right], \end{aligned} \quad (54)$$

$$\begin{aligned} \bar{B}_f(\hat{n}|\hat{k}) &= \tilde{h}_+(1 - \cos\theta) \sin 2\phi - \tilde{h}_\times(1 - \cos\theta) \cos 2\phi \\ &= \frac{-i}{\sqrt{2}} \left[\tilde{h}_L^t(1 - \cos\theta) e^{2i\phi} - \tilde{h}_R^t(1 - \cos\theta) e^{-2i\phi} \right], \end{aligned} \quad (55)$$

where we have taken again the coordinates of $\hat{k} = (0, 0, 1)$ and $\hat{n} = (\sin\theta \cos\phi, \sin\theta \sin\phi, \cos\theta)$. We note that the right-hand side of Eq. (54) is the same as Eq. (22) except for the overall factor 2. From this and Eq. (48), we can obtain

$$\begin{aligned} \tilde{E}_{f,\ell m}(\hat{k}) &= \frac{1}{\sqrt{\ell(\ell+1)}} \int d^2\hat{n} Y_{\ell m}^*(\hat{n}) \bar{E}_f(\hat{n}|\hat{k}) \\ &= \frac{E_\ell^t}{\sqrt{2}} \left(\tilde{h}_L^t(f, \hat{k}) \delta_{m2} + \tilde{h}_R^t(f, \hat{k}) \delta_{m,-2} \right), \end{aligned} \quad (56)$$

$$\begin{aligned} \tilde{B}_{f,\ell m}(\hat{k}) &= \frac{1}{\sqrt{\ell(\ell+1)}} \int d^2\hat{n} Y_{\ell m}^*(\hat{n}) \bar{B}_f(\hat{n}|\hat{k}) \\ &= \frac{B_\ell^t}{\sqrt{2}} \left(\tilde{h}_L^t(f, \hat{k}) \delta_{m2} - \tilde{h}_R^t(f, \hat{k}) \delta_{m,-2} \right), \end{aligned} \quad (57)$$

where

$$E_\ell^t \equiv \frac{2(-1)^\ell}{\sqrt{\ell(\ell+1)}} \sqrt{\frac{4\pi(2\ell+1)(\ell-2)!}{(\ell+2)!}} = \frac{2}{\sqrt{\ell(\ell+1)}} z_\ell^t, \quad B_\ell^t \equiv (-i) E_\ell^t. \quad (58)$$

Similar to the redshift response case, we can obtain the expression for GWs propagating in a general direction $\hat{\Omega}$:

$$\tilde{E}_{f,\ell m}(\hat{\Omega}) = \frac{E_\ell^t}{\sqrt{2}} \left(\tilde{h}_L^t(f, \hat{\Omega}) D_{m,2}^{(\ell)} + \tilde{h}_R^t(f, \hat{\Omega}) D_{m,-2}^{(\ell)} \right), \quad (59)$$

$$\tilde{B}_{f,\ell m}(\hat{\Omega}) = \frac{B_\ell^t}{\sqrt{2}} \left(\tilde{h}_L^t(f, \hat{\Omega}) D_{m,2}^{(\ell)} - \tilde{h}_R^t(f, \hat{\Omega}) D_{m,-2}^{(\ell)} \right). \quad (60)$$

We here define $S_{f,\ell m} = \int d^2\hat{\Omega} \tilde{S}_{f,\ell m}(\hat{\Omega})$ ($S \in \{E, B\}$) and obtain

$$\langle E_{f,\ell m}^* E_{f,\ell' m'} \rangle = \frac{E_\ell^t E_{\ell'}^t}{z_\ell^t z_{\ell'}^t} \langle z_{f,\ell m}^* z_{f,\ell' m'} \rangle = \frac{4}{\sqrt{\ell(\ell+1)\ell'(\ell'+1)}} \langle z_{f,\ell m}^* z_{f,\ell' m'} \rangle, \quad (61)$$

$$\begin{aligned} \langle E_{f,\ell m}^* B_{f,\ell' m'} \rangle &= \frac{E_\ell^t B_{\ell'}^t}{2} \int d^2\hat{\Omega} \int d^2\hat{\Omega}' \left[\tilde{h}_L^{t,*}(f, \hat{\Omega}) D_{m,2}^{(\ell)*} + \tilde{h}_R^{t,*}(f, \hat{\Omega}) D_{m,-2}^{(\ell)*} \right] \left[\tilde{h}_L^t(f, \hat{\Omega}') D_{m',2}^{(\ell')} - \tilde{h}_R^t(f, \hat{\Omega}') D_{m',-2}^{(\ell')} \right] \\ &= 2E_\ell^t B_{\ell'}^t I_0^t \sum_{LM} (-1)^{m+L} \sqrt{\pi} \langle \ell(-m)\ell' m' | LM \rangle \\ &\quad \times \left\{ \left[-c_{LM}^{t,I} (1 - X_{\ell\ell'}^L) + c_{LM}^{t,V} X_{\ell\ell'}^L \right] \begin{pmatrix} \ell & \ell' & L \\ -2 & 2 & 0 \end{pmatrix} - \left[c_{LM}^{t,E} (1 - X_{\ell\ell'}^L) + i c_{LM}^{t,B} X_{\ell\ell'}^L \right] \begin{pmatrix} \ell & \ell' & L \\ 2 & 2 & -4 \end{pmatrix} \right\}, \end{aligned} \quad (62)$$

$$\begin{aligned} \langle B_{f,\ell m}^* E_{f,\ell' m'} \rangle &= \frac{B_\ell^{t*} E_{\ell'}^t}{2} \int d^2\hat{\Omega} \int d^2\hat{\Omega}' \left[\tilde{h}_L^{t,*}(f, \hat{\Omega}) D_{m,2}^{(\ell)*} - \tilde{h}_R^{t,*}(f, \hat{\Omega}) D_{m,-2}^{(\ell)*} \right] \left[\tilde{h}_L^t(f, \hat{\Omega}') D_{m',2}^{(\ell')} + \tilde{h}_R^t(f, \hat{\Omega}') D_{m',-2}^{(\ell')} \right] \\ &= 2B_\ell^{t*} E_{\ell'}^t I_0^t \sum_{LM} (-1)^{m+L} \sqrt{\pi} \langle \ell(-m)\ell' m' | LM \rangle \\ &\quad \times \left\{ \left[-c_{LM}^{t,I} (1 - X_{\ell\ell'}^L) + c_{LM}^{t,V} X_{\ell\ell'}^L \right] \begin{pmatrix} \ell & \ell' & L \\ -2 & 2 & 0 \end{pmatrix} + \left[c_{LM}^{t,E} (1 - X_{\ell\ell'}^L) + i c_{LM}^{t,B} X_{\ell\ell'}^L \right] \begin{pmatrix} \ell & \ell' & L \\ 2 & 2 & -4 \end{pmatrix} \right\}, \end{aligned} \quad (63)$$

$$\begin{aligned} \langle B_{f,\ell m}^* B_{f,\ell' m'} \rangle &= \frac{B_\ell^{t*} B_{\ell'}^t}{2} \int d^2\hat{\Omega} \int d^2\hat{\Omega}' \left[\tilde{h}_L^{t,*}(f, \hat{\Omega}) D_{m,2}^{(\ell)*} - \tilde{h}_R^{t,*}(f, \hat{\Omega}) D_{m,-2}^{(\ell)*} \right] \left[\tilde{h}_L^t(f, \hat{\Omega}') D_{m',2}^{(\ell')} - \tilde{h}_R^t(f, \hat{\Omega}') D_{m',-2}^{(\ell')} \right] \\ &= 2B_\ell^{t*} B_{\ell'}^t I_0^t \sum_{LM} (-1)^{m+L} \sqrt{\pi} \langle \ell(-m)\ell' m' | LM \rangle \\ &\quad \times \left\{ \left[c_{LM}^{t,I} X_{\ell\ell'}^L - c_{LM}^{t,V} (1 - X_{\ell\ell'}^L) \right] \begin{pmatrix} \ell & \ell' & L \\ -2 & 2 & 0 \end{pmatrix} - \left[c_{LM}^{t,E} X_{\ell\ell'}^L + i c_{LM}^{t,B} (1 - X_{\ell\ell'}^L) \right] \begin{pmatrix} \ell & \ell' & L \\ 2 & 2 & -4 \end{pmatrix} \right\}, \end{aligned} \quad (64)$$

where see Eq. (33) for the expression of $\langle z_{f,\ell m}^* z_{f,\ell' m'} \rangle$ due to spin-2 GWs.

From these, the ORF coefficients are

$$F_{\ell\ell'}^{L,t,X,EE} = \frac{4}{\sqrt{\ell(\ell+1)\ell'(\ell'+1)}} F_{\ell\ell'}^{L,t,X,zz}, \quad (65)$$

and the left column in Tables II for $F_{\ell\ell'}^{L,t,X,EB}$, III for $F_{\ell\ell'}^{L,t,X,BE}$, and IV for $F_{\ell\ell'}^{L,t,X,BB}$. To get the concrete plots of the ORFs, we similarly take the coordinates given in Eq. (34). Strictly speaking, in that choice of coordinates, $Y_{(\ell m)\phi}^E(\hat{n}_a)$ and $Y_{(\ell m)\theta}^B(\hat{n}_a)$ are not well defined because of $\sin\theta$ in the denominator, which is from the singularity of the coordinates. To avoid this issue, we define $Y_{(\ell m)\phi}^E(\hat{n}_a)$ and $Y_{(\ell m)\theta}^B(\hat{n}_a)$ with $\hat{n}_a = \hat{n}_b|_{\theta \rightarrow +0}$ in the coordinates. Practically, we take $\hat{n}_a = (\sin\theta_\epsilon, 0, \cos\theta_\epsilon)$ with $\theta_\epsilon = 10^{-5}$ in the numerical calculation for Figs. 3-6. Then, Figure 3 shows the θ -dependence of $\Gamma_{LM}^{t,I,EB}$. In the figure, we can see $\Gamma_{00}^{t,I,EB} = 0$. This physically means that the parity-breaking signal (EB -correlation) cannot be produced in the parity-conserving background (isotropic and unpolarized background).

2. Spin-1 GWs

Next, we discuss the deflection due to spin-1 GWs. From Eqs. (49) and (50), the deflection due to the spin-1 GWs with the frequency f and the propagation direction \hat{k} becomes

$$\begin{aligned} \bar{E}(\hat{n}|\hat{k}) &= \tilde{h}_x \frac{(\sin 2\theta + \sin\theta) \cos\phi}{1 + \cos\theta} + \tilde{h}_y \frac{(\sin 2\theta + \sin\theta) \sin\phi}{1 + \cos\theta} \\ &= \frac{1}{\sqrt{2}} \left[\tilde{h}_L^v \frac{(\sin 2\theta + \sin\theta)}{1 + \cos\theta} e^{i\phi} + \tilde{h}_R^v \frac{(\sin 2\theta + \sin\theta)}{1 + \cos\theta} e^{-i\phi} \right], \\ \bar{B}(\hat{n}|\hat{k}) &= \tilde{h}_x \frac{\sin 2\theta \sin\phi}{2(1 + \cos\theta)} - \tilde{h}_y \frac{\sin 2\theta \cos\phi}{2(1 + \cos\theta)} \end{aligned} \quad (66)$$

X	Spin-2	Spin-1
I	$-2E_\ell^t B_{\ell'}^t \begin{pmatrix} \ell & \ell' & L \\ -2 & 2 & 0 \end{pmatrix} (1 - X_{\ell\ell'}^L)$	$2E_\ell^v B_{\ell'}^v \begin{pmatrix} \ell & \ell' & L \\ -1 & 1 & 0 \end{pmatrix} (1 - X_{\ell\ell'}^L)$
V	$2E_\ell^t B_{\ell'}^t \begin{pmatrix} \ell & \ell' & L \\ -2 & 2 & 0 \end{pmatrix} X_{\ell\ell'}^L$	$-2E_\ell^v B_{\ell'}^v \begin{pmatrix} \ell & \ell' & L \\ -1 & 1 & 0 \end{pmatrix} X_{\ell\ell'}^L$
E	$-2E_\ell^t B_{\ell'}^t \begin{pmatrix} \ell & \ell' & L \\ 2 & 2 & -4 \end{pmatrix} (1 - X_{\ell\ell'}^L)$	$-2E_\ell^v B_{\ell'}^v \begin{pmatrix} \ell & \ell' & L \\ 1 & 1 & -2 \end{pmatrix} (1 - X_{\ell\ell'}^L)$
B	$-2E_\ell^t B_{\ell'}^t \begin{pmatrix} \ell & \ell' & L \\ 2 & 2 & -4 \end{pmatrix} X_{\ell\ell'}^L$	$-2E_\ell^v B_{\ell'}^v \begin{pmatrix} \ell & \ell' & L \\ 1 & 1 & -2 \end{pmatrix} X_{\ell\ell'}^L$

TABLE II. The summary of $F_{\ell\ell'}^{L,p,X,EB}$. See Eq. (58) for E_ℓ^t and $B_{\ell'}^t$ and Eq. (70) for E_ℓ^v and $B_{\ell'}^v$.

X	Spin-2	Spin-1
I	$-2B_\ell^{t*} E_{\ell'}^t \begin{pmatrix} \ell & \ell' & L \\ -2 & 2 & 0 \end{pmatrix} (1 - X_{\ell\ell'}^L)$	$2B_\ell^{v*} E_{\ell'}^v \begin{pmatrix} \ell & \ell' & L \\ -1 & 1 & 0 \end{pmatrix} (1 - X_{\ell\ell'}^L)$
V	$2B_\ell^{t*} E_{\ell'}^t \begin{pmatrix} \ell & \ell' & L \\ -2 & 2 & 0 \end{pmatrix} X_{\ell\ell'}^L$	$-2B_\ell^{v*} E_{\ell'}^v \begin{pmatrix} \ell & \ell' & L \\ -1 & 1 & 0 \end{pmatrix} X_{\ell\ell'}^L$
E	$2B_\ell^{t*} E_{\ell'}^t \begin{pmatrix} \ell & \ell' & L \\ 2 & 2 & -4 \end{pmatrix} (1 - X_{\ell\ell'}^L)$	$2B_\ell^{v*} E_{\ell'}^v \begin{pmatrix} \ell & \ell' & L \\ 1 & 1 & -2 \end{pmatrix} (1 - X_{\ell\ell'}^L)$
B	$2B_\ell^{t*} E_{\ell'}^t \begin{pmatrix} \ell & \ell' & L \\ 2 & 2 & -4 \end{pmatrix} X_{\ell\ell'}^L$	$2B_\ell^{v*} E_{\ell'}^v \begin{pmatrix} \ell & \ell' & L \\ 1 & 1 & -2 \end{pmatrix} X_{\ell\ell'}^L$

TABLE III. The summary of $F_{\ell\ell'}^{L,p,X,BE}$.

X	Spin-2	Spin-1
I	$2B_\ell^{t*} B_{\ell'}^t \begin{pmatrix} \ell & \ell' & L \\ -2 & 2 & 0 \end{pmatrix} X_{\ell\ell'}^L$	$-2B_\ell^{v*} B_{\ell'}^v \begin{pmatrix} \ell & \ell' & L \\ -1 & 1 & 0 \end{pmatrix} X_{\ell\ell'}^L$
V	$-2B_\ell^{t*} B_{\ell'}^t \begin{pmatrix} \ell & \ell' & L \\ -2 & 2 & 0 \end{pmatrix} (1 - X_{\ell\ell'}^L)$	$2B_\ell^{v*} B_{\ell'}^v \begin{pmatrix} \ell & \ell' & L \\ -1 & 1 & 0 \end{pmatrix} (1 - X_{\ell\ell'}^L)$
E	$-2B_\ell^{t*} B_{\ell'}^t \begin{pmatrix} \ell & \ell' & L \\ 2 & 2 & -4 \end{pmatrix} X_{\ell\ell'}^L$	$-2B_\ell^{v*} B_{\ell'}^v \begin{pmatrix} \ell & \ell' & L \\ 1 & 1 & -2 \end{pmatrix} X_{\ell\ell'}^L$
B	$-2B_\ell^{t*} B_{\ell'}^t \begin{pmatrix} \ell & \ell' & L \\ 2 & 2 & -4 \end{pmatrix} (1 - X_{\ell\ell'}^L)$	$-2B_\ell^{v*} B_{\ell'}^v \begin{pmatrix} \ell & \ell' & L \\ 1 & 1 & -2 \end{pmatrix} (1 - X_{\ell\ell'}^L)$

TABLE IV. The summary of $F_{\ell\ell'}^{L,p,X,BB}$.

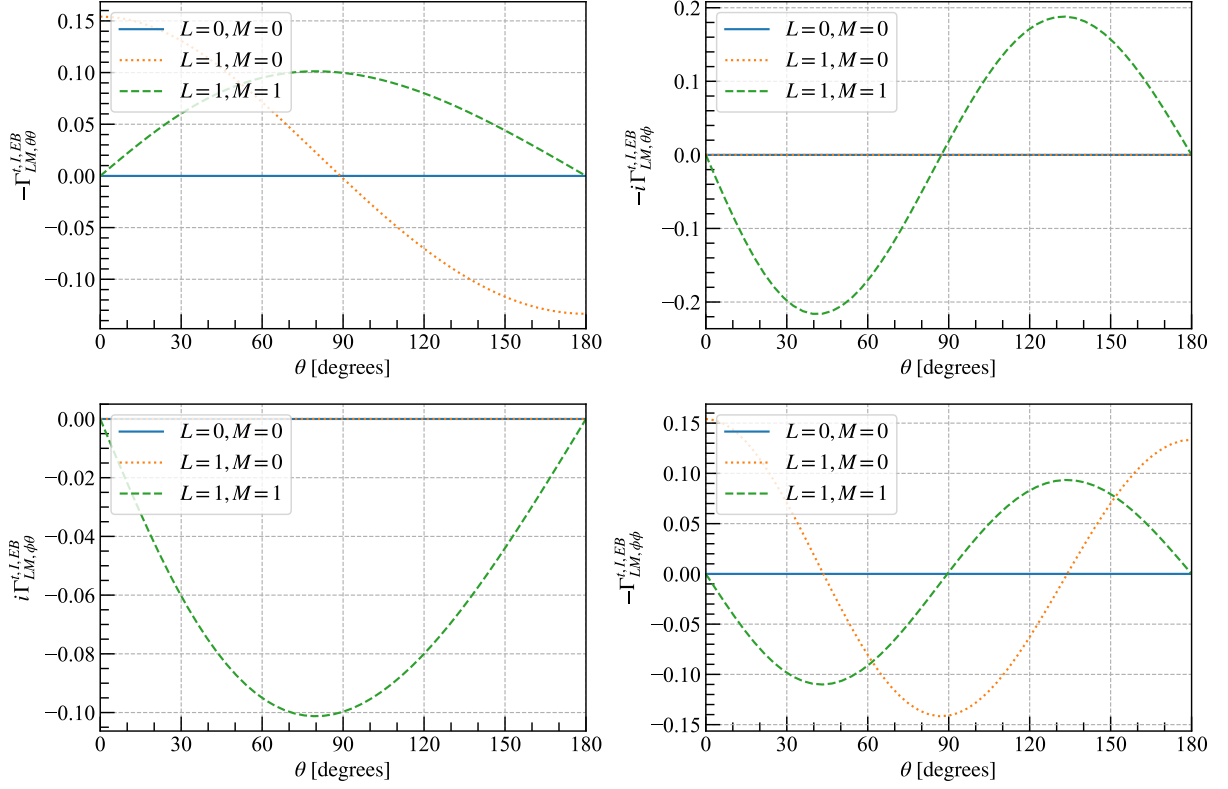


FIG. 3. The ORFs of $\Gamma_{LM}^{t,I,EB}(\theta)$ with $\ell_{\max} = 10$.

$$= \frac{1}{2\sqrt{2}}(-i) \left[\tilde{h}_L^v \frac{\sin 2\theta}{1 + \cos \theta} e^{i\phi} - \tilde{h}_R^v \frac{\sin 2\theta}{1 + \cos \theta} e^{-i\phi} \right]. \quad (67)$$

We here note that Eq. (67) is the same as Eq. (35) except for the relative sign between the two terms and the overall $(-i)$. Then, we obtain

$$\begin{aligned} \tilde{E}_{f,\ell m}(\hat{k}) &= \frac{1}{\sqrt{\ell(\ell+1)}} \int_0^{2\pi} d\phi \int_0^\theta d\theta \sin \theta Y_{\ell m}^*(\theta, \phi) \bar{E}(\hat{n}|\hat{k}) \\ &= \frac{E_\ell^v}{\sqrt{2}} \left(\tilde{h}_L^v(f, \hat{k}) \delta_{m1} - \tilde{h}_R^v(f, \hat{k}) \delta_{m,-1} \right), \end{aligned} \quad (68)$$

$$\begin{aligned} \tilde{B}_{f,\ell m}(\hat{k}) &= \frac{1}{\sqrt{\ell(\ell+1)}} \int_0^{2\pi} d\phi \int_0^\theta d\theta \sin \theta Y_{\ell m}^*(\theta, \phi) \bar{B}(\hat{n}|\hat{k}) \\ &= \frac{B_\ell^v}{\sqrt{2}} \left(\tilde{h}_L^v(f, \hat{k}) \delta_{m1} + \tilde{h}_R^v(f, \hat{k}) \delta_{m,-1} \right), \end{aligned} \quad (69)$$

where

$$E_\ell^v \equiv (-1)^{\ell+1} \sqrt{\frac{4\pi(2\ell+1)}{\ell(\ell+1)}} \left(\frac{1}{\sqrt{\ell(\ell+1)}} - \frac{2\sqrt{2}}{3} \delta_{\ell 1} \right), \quad B_\ell^v \equiv \frac{-i}{\sqrt{\ell(\ell+1)}} z_\ell^v. \quad (70)$$

We can calculate the ORF coefficients in the same way as the spin-1 case for the redshift response. Similar to the previous cases, we can obtain the expression for GWs propagating in a general direction $\hat{\Omega}$:

$$\tilde{E}_{f,\ell m}(\hat{\Omega}) = \frac{E_\ell^v}{\sqrt{2}} \left(\tilde{h}_L^v(f, \hat{\Omega}) D_{m',1}^{(\ell')} - \tilde{h}_R^v(f, \hat{\Omega}) D_{m',-1}^{(\ell')} \right), \quad (71)$$

$$\tilde{B}_{f,\ell m}(\hat{\Omega}) = \frac{B_\ell^v}{\sqrt{2}} \left(\tilde{h}_L^v(f, \hat{\Omega}) D_{m',1}^{(\ell')} + \tilde{h}_R^v(f, \hat{\Omega}) D_{m',-1}^{(\ell')} \right). \quad (72)$$

Note that Eq. (66) has the same structure as Eq. (38) with $z_\ell^v \rightarrow E_\ell^v$. We here define $S_{f,\ell m} = \int d^2\hat{\Omega} \tilde{S}_{f,\ell m}(\hat{\Omega})$ ($S \in \{E, B\}$) and obtain

$$\langle E_{f,\ell m}^* E_{f,\ell' m'} \rangle = \frac{E_\ell^v E_{\ell'}^v}{z_\ell^v z_{\ell'}^v} \langle z_{f,\ell m}^* z_{f,\ell' m'} \rangle, \quad (73)$$

$$\begin{aligned} \langle E_{f,\ell m}^* B_{f,\ell' m'} \rangle &= \frac{E_\ell^v B_{\ell'}^v}{2} \int d^2\hat{\Omega} \int d^2\hat{\Omega}' \left[\tilde{h}_L^{v,*}(f, \hat{\Omega}) D_{m,1}^{(\ell)*} - \tilde{h}_R^{v,*}(f, \hat{\Omega}) D_{m,-1}^{(\ell)*} \right] \left[\tilde{h}_L^v(f, \hat{\Omega}') D_{m',1}^{(\ell')} + \tilde{h}_R^v(f, \hat{\Omega}') D_{m',-1}^{(\ell')} \right] \\ &= 2E_\ell^v B_{\ell'}^v I_0^v \sum_{LM} (-1)^{m+L} \sqrt{\pi} \langle \ell(-m)\ell' m' | LM \rangle \\ &\quad \times \left\{ \left[c_{LM}^{v,I} (1 - X_{\ell\ell'}^L) - c_{LM}^{v,V} X_{\ell\ell'}^L \right] \begin{pmatrix} \ell & \ell' & L \\ -1 & 1 & 0 \end{pmatrix} + \left[-c_{LM}^{v,E} (1 - X_{\ell\ell'}^L) - i c_{LM}^{v,B} X_{\ell\ell'}^L \right] \begin{pmatrix} \ell & \ell' & L \\ 1 & 1 & -2 \end{pmatrix} \right\}, \end{aligned} \quad (74)$$

$$\begin{aligned} \langle B_{f,\ell m}^* E_{f,\ell' m'} \rangle &= \frac{B_\ell^{v*} E_{\ell'}^v}{2} \int d^2\hat{\Omega} \int d^2\hat{\Omega}' \left[\tilde{h}_L^{v,*}(f, \hat{\Omega}) D_{m,1}^{(\ell)*} + \tilde{h}_R^{v,*}(f, \hat{\Omega}) D_{m,-1}^{(\ell)*} \right] \left[\tilde{h}_L^v(f, \hat{\Omega}') D_{m',1}^{(\ell')} - \tilde{h}_R^v(f, \hat{\Omega}') D_{m',-1}^{(\ell')} \right] \\ &= 2B_\ell^{v*} E_{\ell'}^v I_0^v \sum_{LM} (-1)^{m+L} \sqrt{\pi} \langle \ell(-m)\ell' m' | LM \rangle \\ &\quad \times \left\{ \left[c_{LM}^{v,I} (1 - X_{\ell\ell'}^L) - c_{LM}^{v,V} X_{\ell\ell'}^L \right] \begin{pmatrix} \ell & \ell' & L \\ -1 & 1 & 0 \end{pmatrix} + \left[c_{LM}^{v,E} (1 - X_{\ell\ell'}^L) + i c_{LM}^{v,B} X_{\ell\ell'}^L \right] \begin{pmatrix} \ell & \ell' & L \\ 1 & 1 & -2 \end{pmatrix} \right\}, \end{aligned} \quad (75)$$

$$\begin{aligned} \langle B_{f,\ell m}^* B_{f,\ell' m'} \rangle &= \frac{B_\ell^{v*} B_{\ell'}^v}{2} \int d^2\hat{\Omega} \int d^2\hat{\Omega}' \left[\tilde{h}_L^{v,*}(f, \hat{\Omega}) D_{m,1}^{(\ell)*} + \tilde{h}_R^{v,*}(f, \hat{\Omega}) D_{m,-1}^{(\ell)*} \right] \left[\tilde{h}_L^v(f, \hat{\Omega}') D_{m',1}^{(\ell')} + \tilde{h}_R^v(f, \hat{\Omega}') D_{m',-1}^{(\ell')} \right] \\ &= 2B_\ell^{v*} B_{\ell'}^v I_0^v \sum_{LM} (-1)^{m+L} \sqrt{\pi} \langle \ell(-m)\ell' m' | LM \rangle \\ &\quad \times \left\{ \left[-c_{LM}^{v,I} X_{\ell\ell'}^L + c_{LM}^{v,V} (1 - X_{\ell\ell'}^L) \right] \begin{pmatrix} \ell & \ell' & L \\ -1 & 1 & 0 \end{pmatrix} + \left[-c_{LM}^{v,E} X_{\ell\ell'}^L - i c_{LM}^{v,B} (1 - X_{\ell\ell'}^L) \right] \begin{pmatrix} \ell & \ell' & L \\ 1 & 1 & -2 \end{pmatrix} \right\}, \end{aligned} \quad (76)$$

where see Eq. (39) for the expression of $\langle z_{f,\ell m}^* z_{f,\ell' m'} \rangle$ due to spin-1 GWs. From this, the ORF coefficients are

$$F_{\ell\ell'}^{L,v,X,EE} = \frac{E_\ell^v E_{\ell'}^v}{z_\ell^v z_{\ell'}^v} F_{\ell\ell'}^{L,v,X,zz}, \quad (77)$$

and the right column in Tables II for $F_{\ell\ell'}^{L,v,X,EB}$, III for $F_{\ell\ell'}^{L,v,X,BE}$, and IV for $F_{\ell\ell'}^{L,v,X,BB}$. Figure 4 shows the result of $\Gamma_{LM}^{v,I,EB}$. In the figure, we can see again $\Gamma_{00}^{v,I,EB} = 0$, similar to the spin-2 GW case (Fig. 3).

C. Cross-correlation between redshift response and deflection fields

We finally discuss the cross-correlation between the redshift response and the angular deflection. We here consider the two-point correlation function of z and $\delta\vec{n}$:

$$\begin{aligned} \langle z_f^*(\hat{n}_a) \delta n_{f,i}(\hat{n}_b) \rangle &= \sum_{\ell m} \sum_{\ell' m'} \sum_S \langle z_{f,\ell m}^* S_{f,\ell' m'} \rangle Y_{\ell m}^*(\hat{n}_a) Y_{(\ell' m'),i}^S(\hat{n}_b) \\ &= \sum_{p=t,v} \sum_X \sum_S i^X \left[I_0^p \sum_{L,M} c_{LM}^{p,X} \Gamma_{LM,i}^{p,X,z^S}(\hat{n}_a, \hat{n}_b) \right], \end{aligned} \quad (78)$$

$$\begin{aligned} \langle \delta n_{f,i}^*(\hat{n}_a) z_f(\hat{n}_b) \rangle &= \sum_{\ell m} \sum_{\ell' m'} \sum_S \langle S_{f,\ell m}^* z_{f,\ell' m'} \rangle Y_{(\ell m),i}^{S*}(\hat{n}_a) Y_{\ell' m'}(\hat{n}_b) \\ &= \sum_{p=t,v} \sum_X \sum_S i^X \left[I_0^p \sum_{L,M} c_{LM}^{p,X} \Gamma_{LM,i}^{p,X,Sz}(\hat{n}_a, \hat{n}_b) \right], \end{aligned} \quad (79)$$

where $S \in \{E, B\}$. The ORFs are given by

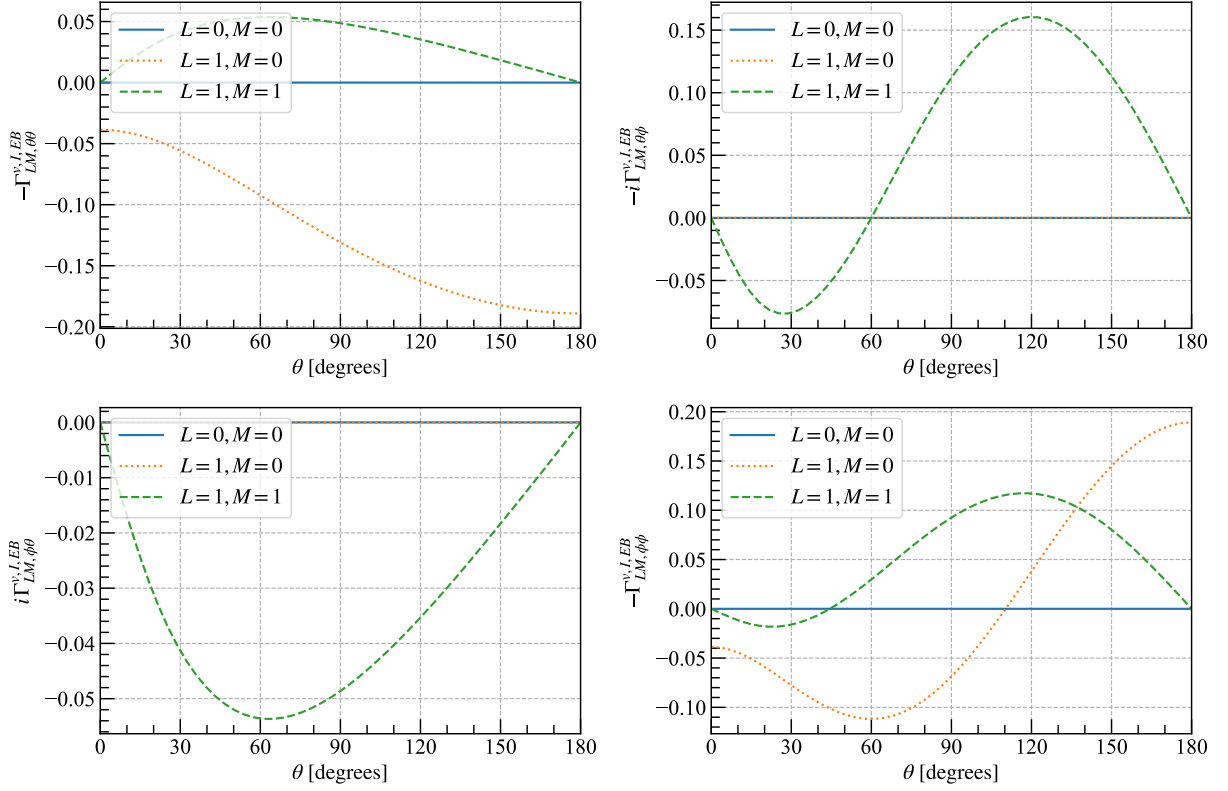


FIG. 4. The ORFs of $\Gamma_{LM}^{v,I,EB}(\theta)$ with $\ell_{\max} = 10$.

$$\Gamma_{(LM)i}^{p,X,zS}(\hat{n}_a, \hat{n}_b) = (-1)^L \sqrt{\pi} \sum_{\ell=\ell_{\min}}^{\ell_{\max}} \sum_{\ell'=\ell_{\min}}^{\ell_{\max}} F_{\ell\ell'}^{L,p,X,zS} \left\{ Y_{\ell}(\hat{n}_a) \otimes Y_{(\ell')i}^S(\hat{n}_b) \right\}_{LM}, \quad (80)$$

$$\Gamma_{(LM)i}^{p,X,Sz}(\hat{n}_a, \hat{n}_b) = (-1)^L \sqrt{\pi} \sum_{\ell=\ell_{\min}}^{\ell_{\max}} \sum_{\ell'=\ell_{\min}}^{\ell_{\max}} F_{\ell\ell'}^{L,p,X,Sz} \left\{ Y_{(\ell)i}^S(\hat{n}_a) \otimes Y_{\ell'}(\hat{n}_b) \right\}_{LM}, \quad (81)$$

where

$$\left\{ Y_{\ell}(\hat{n}_a) \otimes Y_{(\ell')i}^S(\hat{n}_b) \right\}_{LM} = \sum_{m=-\ell}^{\ell} \sum_{m'=-\ell'}^{\ell'} \langle \ell m \ell' m' | LM \rangle Y_{\ell m}(\hat{n}_a) Y_{(\ell')m'i}^S(\hat{n}_b), \quad (82)$$

$$\left\{ Y_{(\ell)i}^S(\hat{n}_a) \otimes Y_{\ell'}(\hat{n}_b) \right\}_{LM} = \sum_{m=-\ell}^{\ell} \sum_{m'=-\ell'}^{\ell'} \langle \ell m \ell' m' | LM \rangle Y_{(\ell)m}^S(\hat{n}_a) Y_{\ell' m'}(\hat{n}_b). \quad (83)$$

We here recall that the redshift responses Eqs. (26) (for spin-2 GWs) and (38) (for spin-1 GWs) are the same as the E-mode angular deflection Eqs. (59) and (71) with $z_{\ell}^p \rightarrow E_{\ell}^p$, respectively. From this, we can obtain the following relations for the ORF coefficients:

$$F_{\ell\ell'}^{L,p,X,zS} = \frac{z_{\ell}^p}{E_{\ell}^p} F_{\ell\ell'}^{L,p,X,ES}, \quad F_{\ell\ell'}^{L,p,X,Sz} = \frac{z_{\ell'}^p}{E_{\ell'}^p} F_{\ell\ell'}^{L,p,X,SE}. \quad (84)$$

Figures 5 and 6 show the θ dependence of $\Gamma_{LM}^{t,I,Ez}$ and $\Gamma_{LM}^{v,I,Ez}$, respectively.

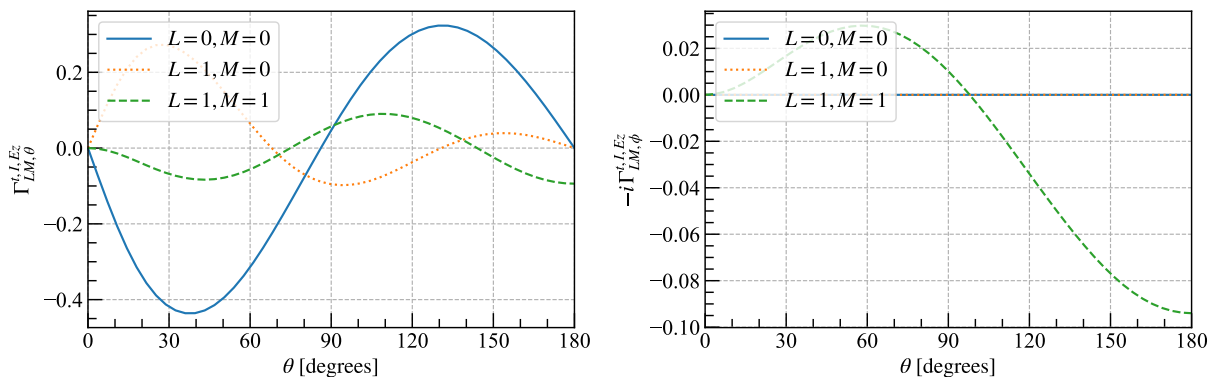


FIG. 5. The ORFs of $\Gamma_{LM}^{t,I,Ez}(\theta)$ with $\ell_{\max} = 10$.

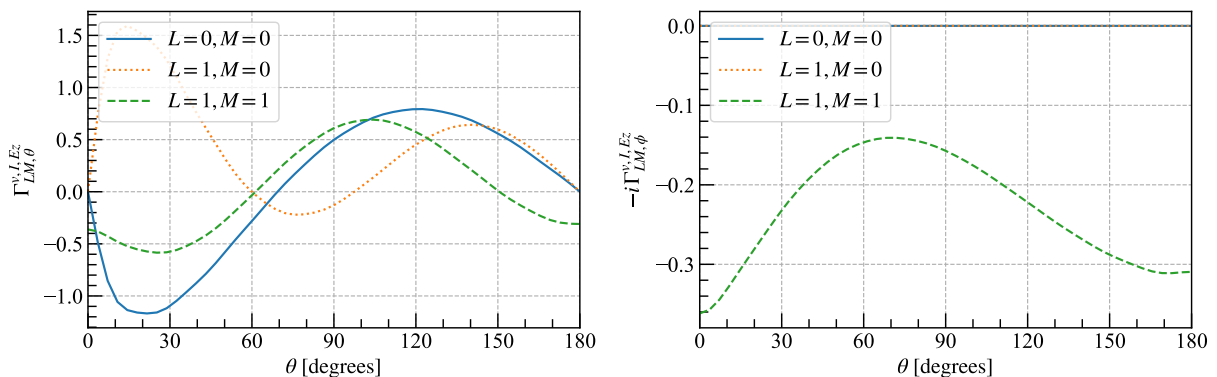


FIG. 6. The ORFs of $\Gamma_{LM}^{v,I,Ez}(\theta)$ with $\ell_{\max} = 20$.

IV. CONCLUSION

Here we have shown how to calculate the most general two-point correlation functions (or ORFs) for PTA timing residuals and the two components of the astrometric deflection due to a SGWB characterized by an arbitrary intensity and linear/circular-polarization pattern on the sky. Results were presented for both the spin-2 (tensor) GWs that appear in general relativity as well as spin-1 (vector) GWs that may appear in alternative-gravity theories.

We have checked that our results for PTA timing residuals for an anisotropic, unpolarized, spin-2 and spin-1 GW background agree with Ref. [50] up to $L \leq 3$. (While we have verified that our results are consistent for $L \leq 3$, we have only plotted up to $L \leq 1$.) For an anisotropic, polarized (either circular or linear) GW background, our results agree with those in Ref. [45]. For astrometric angular deflections with $L = M = 0$ with spin-2 and spin-1 GW background, our results correspond with those in Refs. [24–26, 46, 47]. The results presented here for astrometry with $L \geq 1$ are new. Note that we show only a limited number of plots in this paper and refer to [our Github page](#) for the other ORFs.

These computations are a first step that can be followed in subsequent work on detection forecasts, mission concept studies, and observational strategies. We also leave the construction of estimators from astrometric deflections for anisotropy/polarization to future work, although they should follow analogous prior work. And finally, we have restricted the calculation of the $F_{\ell\ell'}^L$ coefficients in the BiPoSH expansions of the ORFs to GWs that propagate at the speed of light. It may be interesting to generalize in future work to nonluminal modes.

ACKNOWLEDGEMENTS

This work was supported at Johns Hopkins by NSF Grant No. 2112699, the Simons Foundation, and the Templeton Foundation. K.I. acknowledges the support of JSPS Postdoctoral Fellowships for Research Abroad. C.T. acknowledges the support of the Department of Education Award #P382G170104 (TITLE-VII). S.R.T. acknowledges support from

NSF AST-2007993, NSF AST-2307719, and an NSF CAREER #2146016. S.R.T. is a member of the NANOGrav collaboration, which receives support from NSF Physics Frontiers Center award number 1430284 and 2020265. Any opinions, findings, interpretations, conclusions, or recommendations expressed in this material are those of its authors and do not represent the views of the Department of Education.

Appendix A: Wigner D -matrix

In this Appendix, we summarize the properties of the Wigner D -matrix. We consider the rotation of the coordinates:

$$\hat{n}^i \rightarrow \hat{n}'^i = R^{ij} \hat{n}_j, \quad (\text{A1})$$

where R^{ij} is the rotation matrix given by [60]

$$R = \begin{pmatrix} \cos \alpha \cos \beta \cos \gamma - \sin \alpha \sin \gamma & -\cos \alpha \cos \beta \sin \gamma - \sin \alpha \cos \gamma & \cos \alpha \sin \beta \\ \sin \alpha \cos \beta \cos \gamma + \cos \alpha \sin \gamma & -\sin \alpha \cos \beta \sin \gamma + \cos \alpha \cos \gamma & \sin \alpha \sin \beta \\ -\sin \beta \cos \gamma & \sin \beta \sin \gamma & \cos \beta \end{pmatrix}, \quad (\text{A2})$$

where α , β , and γ are the Euler angles in the z - y - z notation. In this transformation, the spherical harmonics in the two coordinates are related to the Wigner D -matrix as [62]

$$Y_{\ell m}(\hat{n}') = \sum_{m'} Y_{\ell m'}(\hat{n}) D_{m'm}^{(\ell)}(R^{-1}), \quad (\text{A3})$$

where R^{-1} is the inverse rotation of R . We here express Wigner D -matrix as³

$$D_{mm'}^{(\ell)}(R) = D_{mm'}^{(\ell)}(\alpha, \beta, \gamma), \quad D_{m'm}^{(\ell)}(R^{-1}) = D_{m'm}^{(\ell)}(-\gamma, -\beta, -\alpha). \quad (\text{A4})$$

Also, its complex conjugate is given by [60]

$$D_{mm'}^{(\ell)*}(R) = (-1)^{m'-m} D_{-m-m'}^{(\ell)}(R). \quad (\text{A5})$$

The spin-weighted spherical harmonic is related to Wigner D -matrix as [50, 63, 64]⁴

$${}_s Y_{\ell m}(\theta, \phi) = (-1)^m \sqrt{\frac{2\ell+1}{4\pi}} D_{-ms}^{(\ell)}(\phi, \theta, \gamma) e^{is\gamma}. \quad (\text{A6})$$

Wigner D -matrix can be expressed with Wigner small d -matrix $d_{mm'}^{\ell}(\beta)$,

$$D_{mm'}^{(\ell)}(\alpha, \beta, \gamma) = e^{-im\alpha} d_{mm'}^{\ell}(\beta) e^{-im'\gamma}. \quad (\text{A7})$$

Using $d_{mm'}^{\ell*}(\beta) = d_{m'm}^{\ell}(-\beta)$, we can see that Wigner D -matrix satisfies the following relation:

$$D_{m'm}^{(\ell)}(R^{-1}) = D_{mm'}^{(\ell)*}(R). \quad (\text{A8})$$

Using this, we can reexpress Eq. (A9) as

$$Y_{\ell m}(\hat{n}') = \sum_{m'} D_{mm'}^{(\ell)*}(\alpha, \beta, \gamma) Y_{\ell m'}(\hat{n}). \quad (\text{A9})$$

In the main text (e.g. Eq. (25)), we consider the transformation from the coordinates where the z -axis is aligned with the GW propagation direction ($\hat{k} \parallel \hat{z}$) to general coordinates. Let us here relate the angular coefficients in the two coordinates by using the above expressions. In general, we can expand some function of \hat{n} as

$$f(\hat{n}|\hat{k}) = \sum_{\ell m} \tilde{f}_{\ell m}(\hat{k}) Y_{\ell m}(\hat{n}|\hat{k}), \quad (\text{A10})$$

³ In Ref. [62], Wigner D -matrix is expressed as $D_{m'm}^{(\ell)}(R^{-1}) = D_{m'm}^{(\ell)}(\alpha\beta\gamma)$.

⁴ The normalization of the spin-weighted spherical harmonics is slightly different from that in Ref. [62]. With the normalization of Ref. [62], we find ${}_s Y_{\ell m}(\theta, \phi) = (-1)^{m-s} \sqrt{\frac{2\ell+1}{4\pi}} D_{-ms}^{(\ell)}(\phi, \theta, \gamma) e^{is\gamma}$.

where \hat{n} is defined in the coordinates with \hat{k} aligned along the z -axis. We now move to other coordinates where $\hat{\Omega}(\neq \hat{k})$ is aligned along the z -axis. Even if the physical observation direction is fixed, the coordinate transformation changes the observation direction vector as $\hat{n} \rightarrow \hat{n}'$. That is, we have

$$f(\hat{n}|\hat{k}) = f(\hat{n}'|\hat{\Omega}) = \sum_{\ell m} \tilde{f}_{\ell m}(\hat{k}) Y_{\ell m}(\hat{n}|\hat{k}) = \sum_{\ell m} \tilde{f}_{\ell m}(\hat{\Omega}) Y_{\ell m}(\hat{n}'|\hat{\Omega}). \quad (\text{A11})$$

We here relate $Y_{\ell m}(\hat{n}|\hat{k})$ and $Y_{\ell m}(\hat{n}'|\hat{\Omega})$ using Wigner D -matrix. We here define R as

$$\hat{k}^i = R^{ij} \hat{\Omega}_j. \quad (\text{A12})$$

The Euler angles are $\alpha = \phi_k$ and $\beta = \theta_k$, where $\hat{k} = (\sin \theta_k \cos \phi_k, \sin \theta_k \sin \phi_k, \cos \theta_k)$ in the $\hat{\Omega} \parallel \hat{z}$ coordinates. The final Euler angle γ is arbitrary and we take $\gamma = 0$ in this work, which corresponds to make the polarization of ‘+’, ‘ \times ’, ‘ x ’, and ‘ y ’ aligned with $\hat{\theta}$ and $\hat{\phi}$ directions [40]. Then, we obtain

$$\hat{n}^i = (R^{-1})^{ij} \hat{n}'_j. \quad (\text{A13})$$

Using this and Eq. (A9), we obtain

$$\begin{aligned} Y_{\ell m}(\hat{n}|\hat{k}) &= \sum_{m'} D_{mm'}^{(\ell)*}(R^{-1}) Y_{\ell m'}(\hat{n}'|\hat{\Omega}) \\ &= \sum_{m'} Y_{\ell m'}(\hat{n}'|\hat{\Omega}) D_{m'm}^{(\ell)}(R). \end{aligned} \quad (\text{A14})$$

Substituting this into Eq. (A11), we finally obtain

$$f(\hat{n}'|\hat{\Omega}) = \sum_{\ell} \sum_{mm'} Y_{\ell m}(\hat{n}'|\hat{\Omega}) D_{mm'}^{(\ell)}(\phi_k, \theta_k, 0) \tilde{f}_{\ell m'}(\hat{k}). \quad (\text{A15})$$

This corresponds to the relation in Eq. (25).

-
- [1] G. Agazie *et al.* (NANOGrav), The NANOGrav 15 yr Data Set: Evidence for a Gravitational-wave Background, *Astrophys. J. Lett.* **951**, L8 (2023), [arXiv:2306.16213 \[astro-ph.HE\]](#).
- [2] J. Antoniadis *et al.* (EPTA, InPTA:), The second data release from the European Pulsar Timing Array - III. Search for gravitational wave signals, *Astron. Astrophys.* **678**, A50 (2023), [arXiv:2306.16214 \[astro-ph.HE\]](#).
- [3] D. J. Reardon *et al.*, Search for an Isotropic Gravitational-wave Background with the Parkes Pulsar Timing Array, *Astrophys. J. Lett.* **951**, L6 (2023), [arXiv:2306.16215 \[astro-ph.HE\]](#).
- [4] H. Xu *et al.*, Searching for the Nano-Hertz Stochastic Gravitational Wave Background with the Chinese Pulsar Timing Array Data Release I, *Res. Astron. Astrophys.* **23**, 075024 (2023), [arXiv:2306.16216 \[astro-ph.HE\]](#).
- [5] M. Rajagopal and R. W. Romani, Ultralow frequency gravitational radiation from massive black hole binaries, *Astrophys. J.* **446**, 543 (1995), [arXiv:astro-ph/9412038](#).
- [6] A. H. Jaffe and D. C. Backer, Gravitational waves probe the coalescence rate of massive black hole binaries, *Astrophys. J.* **583**, 616 (2003), [arXiv:astro-ph/0210148](#).
- [7] A. Sesana, A. Vecchio, and C. N. Colacino, The stochastic gravitational-wave background from massive black hole binary systems: implications for observations with Pulsar Timing Arrays, *Mon. Not. Roy. Astron. Soc.* **390**, 192 (2008), [arXiv:0804.4476 \[astro-ph\]](#).
- [8] E. S. Phinney, A Practical theorem on gravitational wave backgrounds, (2001), [arXiv:astro-ph/0108028](#).
- [9] H. Middleton, W. Del Pozzo, W. M. Farr, A. Sesana, and A. Vecchio, Astrophysical constraints on massive black hole binary evolution from Pulsar Timing Arrays, *Mon. Not. Roy. Astron. Soc.* **455**, L72 (2016), [arXiv:1507.00992 \[astro-ph.CO\]](#).
- [10] G. Sato-Polito and M. Kamionkowski, Exploring the spectrum of stochastic gravitational-wave anisotropies with pulsar timing arrays, (2023), [arXiv:2305.05690 \[astro-ph.CO\]](#).
- [11] E. C. Gardiner, L. Z. Kelley, A.-M. Lemke, and A. Mitridate, Beyond the Background: Gravitational Wave Anisotropy and Continuous Waves from Supermassive Black Hole Binaries, (2023), [arXiv:2309.07227 \[astro-ph.HE\]](#).
- [12] G. Sato-Polito, M. Zaldarriaga, and E. Quataert, Where are NANOGrav’s big black holes?, (2023), [arXiv:2312.06756 \[astro-ph.CO\]](#).
- [13] S. Olmez, V. Mandic, and X. Siemens, Gravitational-Wave Stochastic Background from Kinks and Cusps on Cosmic Strings, *Phys. Rev. D* **81**, 104028 (2010), [arXiv:1004.0890 \[astro-ph.CO\]](#).
- [14] L. Sousa and P. P. Avelino, Stochastic Gravitational Wave Background generated by Cosmic String Networks: Velocity-Dependent One-Scale model versus Scale-Invariant Evolution, *Phys. Rev. D* **88**, 023516 (2013), [arXiv:1304.2445 \[astro-ph.CO\]](#).

- [15] K. Miyamoto and K. Nakayama, Cosmological and astrophysical constraints on superconducting cosmic strings, *JCAP* **07**, 012, [arXiv:1212.6687 \[astro-ph.CO\]](#).
- [16] S. Kuroyanaagi, K. Miyamoto, T. Sekiguchi, K. Takahashi, and J. Silk, Forecast constraints on cosmic strings from future CMB, pulsar timing and gravitational wave direct detection experiments, *Phys. Rev. D* **87**, 023522 (2013), [Erratum: *Phys.Rev.D* 87, 069903 (2013)], [arXiv:1210.2829 \[astro-ph.CO\]](#).
- [17] C. Caprini, R. Durrer, and X. Siemens, Detection of gravitational waves from the QCD phase transition with pulsar timing arrays, *Phys. Rev. D* **82**, 063511 (2010), [arXiv:1007.1218 \[astro-ph.CO\]](#).
- [18] A. A. Starobinsky, Spectrum of relict gravitational radiation and the early state of the universe, *JETP Lett.* **30**, 682 (1979).
- [19] W. Zhao, Y. Zhang, X.-P. You, and Z.-H. Zhu, Constraints of relic gravitational waves by pulsar timing arrays: Forecasts for the FAST and SKA projects, *Phys. Rev. D* **87**, 124012 (2013), [arXiv:1303.6718 \[astro-ph.CO\]](#).
- [20] K. Inomata, M. Kawasaki, K. Mukaida, Y. Tada, and T. T. Yanagida, Inflationary primordial black holes for the LIGO gravitational wave events and pulsar timing array experiments, *Phys. Rev. D* **95**, 123510 (2017), [arXiv:1611.06130 \[astro-ph.CO\]](#).
- [21] A. Afzal *et al.* (NANOGrav), The NANOGrav 15 yr Data Set: Search for Signals from New Physics, *Astrophys. J. Lett.* **951**, L11 (2023), [arXiv:2306.16219 \[astro-ph.HE\]](#).
- [22] V. B. Braginsky, N. S. Kardashev, I. D. Novikov, and A. G. Polnarev, Propagation of electromagnetic radiation in a random field of gravitational waves and space radio interferometry, *Nuovo Cim. B* **105**, 1141 (1990).
- [23] N. Kaiser and A. H. Jaffe, Bending of light by gravity waves, *Astrophys. J.* **484**, 545 (1997), [arXiv:astro-ph/9609043](#).
- [24] L. G. Book and E. E. Flanagan, Astrometric Effects of a Stochastic Gravitational Wave Background, *Phys. Rev. D* **83**, 024024 (2011), [arXiv:1009.4192 \[astro-ph.CO\]](#).
- [25] W. Qin, K. K. Boddy, M. Kamionkowski, and L. Dai, Pulsar-timing arrays, astrometry, and gravitational waves, *Phys. Rev. D* **99**, 063002 (2019), [arXiv:1810.02369 \[astro-ph.CO\]](#).
- [26] M. Çalıřkan, Y. Chen, L. Dai, N. Anil Kumar, I. Stomberg, and X. Xue, Dissecting Stochastic Gravitational Wave Background with Astrometry, (2023), [arXiv:2312.03069 \[gr-qc\]](#).
- [27] R. w. Hellings and G. s. Downs, UPPER LIMITS ON THE ISOTROPIC GRAVITATIONAL RADIATION BACKGROUND FROM PULSAR TIMING ANALYSIS, *Astrophys. J.* **265**, L39 (1983).
- [28] J. Darling, A. E. Truebenbach, and J. Paine, Astrometric Limits on the Stochastic Gravitational Wave Background, *Astrophys. J.* **861**, 113 (2018), [arXiv:1804.06986 \[astro-ph.IM\]](#).
- [29] C. Boehm *et al.* (Theia), Theia: Faint objects in motion or the new astrometry frontier, (2017), [arXiv:1707.01348 \[astro-ph.IM\]](#).
- [30] M. A. Fedderke, P. W. Graham, B. Macintosh, and S. Rajendran, Astrometric gravitational-wave detection via stellar interferometry, *Phys. Rev. D* **106**, 023002 (2022), [arXiv:2204.07677 \[astro-ph.IM\]](#).
- [31] Y. Wang, K. Pardo, T.-C. Chang, and O. Doré, Gravitational Wave Detection with Photometric Surveys, *Phys. Rev. D* **103**, 084007 (2021), [arXiv:2010.02218 \[gr-qc\]](#).
- [32] Y. Wang, K. Pardo, T.-C. Chang, and O. Doré, Constraining the stochastic gravitational wave background with photometric surveys, *Phys. Rev. D* **106**, 084006 (2022), [arXiv:2205.07962 \[gr-qc\]](#).
- [33] K. Pardo, T.-C. Chang, O. Doré, and Y. Wang, Gravitational Wave Detection with Relative Astrometry using Roman's Galactic Bulge Time Domain Survey, (2023), [arXiv:2306.14968 \[astro-ph.GA\]](#).
- [34] C. M. F. Mingarelli, T. Sidery, I. Mandel, and A. Vecchio, Characterizing gravitational wave stochastic background anisotropy with pulsar timing arrays, *Phys. Rev. D* **88**, 062005 (2013), [arXiv:1306.5394 \[astro-ph.HE\]](#).
- [35] J. Gair, J. D. Romano, S. Taylor, and C. M. F. Mingarelli, Mapping gravitational-wave backgrounds using methods from CMB analysis: Application to pulsar timing arrays, *Phys. Rev. D* **90**, 082001 (2014), [arXiv:1406.4664 \[gr-qc\]](#).
- [36] S. R. Taylor and J. R. Gair, Searching For Anisotropic Gravitational-wave Backgrounds Using Pulsar Timing Arrays, *Phys. Rev. D* **88**, 084001 (2013), [arXiv:1306.5395 \[gr-qc\]](#).
- [37] G. Agazie *et al.* (NANOGrav), The NANOGrav 15 yr Data Set: Search for Anisotropy in the Gravitational-wave Background, *Astrophys. J. Lett.* **956**, L3 (2023), [arXiv:2306.16221 \[astro-ph.HE\]](#).
- [38] Y.-K. Chu, G.-C. Liu, and K.-W. Ng, Observation of a polarized stochastic gravitational-wave background in pulsar-timing-array experiments, *Phys. Rev. D* **104**, 124018 (2021), [arXiv:2107.00536 \[gr-qc\]](#).
- [39] G.-C. Liu and K.-W. Ng, Timing-residual power spectrum of a polarized stochastic gravitational-wave background in pulsar-timing-array observation, *Phys. Rev. D* **106**, 064004 (2022), [arXiv:2201.06767 \[gr-qc\]](#).
- [40] N. Anil Kumar, M. Çalıřkan, G. Sato-Polito, M. Kamionkowski, and L. Ji, Linear polarization of the stochastic gravitational-wave background with pulsar timing arrays, (2023), [arXiv:2312.03056 \[astro-ph.CO\]](#).
- [41] R. Kato and J. Soda, Probing circular polarization in stochastic gravitational wave background with pulsar timing arrays, *Phys. Rev. D* **93**, 062003 (2016), [arXiv:1512.09139 \[gr-qc\]](#).
- [42] G. Sato-Polito and M. Kamionkowski, Pulsar-timing measurement of the circular polarization of the stochastic gravitational-wave background, *Phys. Rev. D* **106**, 023004 (2022), [arXiv:2111.05867 \[astro-ph.CO\]](#).
- [43] N. Anil Kumar and M. Kamionkowski, All the Pretty Overlap Reduction Functions, (2023), [arXiv:2311.14159 \[astro-ph.CO\]](#).
- [44] N. Anil Kumar, M. Çalıřkan, G. Sato-Polito, M. Kamionkowski, and L. Ji, Linear polarization of the stochastic gravitational-wave background with pulsar timing arrays, (2023), [arXiv:2312.03056 \[astro-ph.CO\]](#).
- [45] R. C. Bernardo, G.-C. Liu, and K.-W. Ng, Correlations for an anisotropic polarized stochastic gravitational wave background in pulsar timing arrays, (2023), [arXiv:2312.03383 \[gr-qc\]](#).
- [46] D. P. Mihaylov, C. J. Moore, J. R. Gair, A. Lasenby, and G. Gilmore, Astrometric Effects of Gravitational Wave Backgrounds with non-Einsteinian Polarizations, *Phys. Rev. D* **97**, 124058 (2018), [arXiv:1804.00660 \[gr-qc\]](#).

- [47] L. O’Beirne and N. J. Cornish, Constraining the Polarization Content of Gravitational Waves with Astrometry, *Phys. Rev. D* **98**, 024020 (2018), [arXiv:1804.03146 \[gr-qc\]](#).
- [48] K. J. Lee, J. F. A., and R. H. Price, Pulsar timing as a probe of non-einsteinian polarizations of gravitational waves, *Astrophys. J.* **685**, 1304 (2008).
- [49] S. J. Chamberlin and X. Siemens, Stochastic backgrounds in alternative theories of gravity: overlap reduction functions for pulsar timing arrays, *Phys. Rev. D* **85**, 082001 (2012), [arXiv:1111.5661 \[astro-ph.HE\]](#).
- [50] J. R. Gair, J. D. Romano, and S. R. Taylor, Mapping gravitational-wave backgrounds of arbitrary polarisation using pulsar timing arrays, *Phys. Rev. D* **92**, 102003 (2015), [arXiv:1506.08668 \[gr-qc\]](#).
- [51] R. W. Hellings and K. Nordtvedt, Vector-Metric Theory of Gravity, *Phys. Rev. D* **7**, 3593 (1973).
- [52] J. Beltran Jimenez and A. L. Maroto, Cosmological evolution in vector-tensor theories of gravity, *Phys. Rev. D* **80**, 063512 (2009), [arXiv:0905.1245 \[astro-ph.CO\]](#).
- [53] N. J. Cornish, L. O’Beirne, S. R. Taylor, and N. Yunes, Constraining alternative theories of gravity using pulsar timing arrays, *Phys. Rev. Lett.* **120**, 181101 (2018), [arXiv:1712.07132 \[gr-qc\]](#).
- [54] D. Jeong and M. Kamionkowski, Clustering Fossils from the Early Universe, *Phys. Rev. Lett.* **108**, 251301 (2012), [arXiv:1203.0302 \[astro-ph.CO\]](#).
- [55] M. Maggiore, *Gravitational Waves. Vol. 2: Astrophysics and Cosmology* (Oxford University Press, 2018).
- [56] A. Hajian and T. Souradeep, Measuring statistical isotropy of the CMB anisotropy, *Astrophys. J. Lett.* **597**, L5 (2003), [arXiv:astro-ph/0308001](#).
- [57] A. Hajian and T. Souradeep, The Cosmic microwave background bipolar power spectrum: Basic formalism and applications, (2005), [arXiv:astro-ph/0501001](#).
- [58] N. Joshi, S. Jhingan, T. Souradeep, and A. Hajian, Bipolar Harmonic encoding of CMB correlation patterns, *Phys. Rev. D* **81**, 083012 (2010), [arXiv:0912.3217 \[astro-ph.CO\]](#).
- [59] L. G. Book, M. Kamionkowski, and T. Souradeep, Odd-Parity Bipolar Spherical Harmonics, *Phys. Rev. D* **85**, 023010 (2012), [arXiv:1109.2910 \[astro-ph.CO\]](#).
- [60] V. K. Khersonskii, A. N. Moskalev, and D. A. Varshalovich, *Quantum Theory Of Angular Momentum* (World Scientific Publishing Company, 1988).
- [61] L. Dai, M. Kamionkowski, and D. Jeong, Total Angular Momentum Waves for Scalar, Vector, and Tensor Fields, *Phys. Rev. D* **86**, 125013 (2012), [arXiv:1209.0761 \[astro-ph.CO\]](#).
- [62] J. N. Goldberg, A. J. MacFarlane, E. T. Newman, F. Rohrlich, and E. C. G. Sudarshan, Spin s spherical harmonics and edth, *J. Math. Phys.* **8**, 2155 (1967).
- [63] T. Okamoto and W. Hu, The angular trispectra of CMB temperature and polarization, *Phys. Rev. D* **66**, 063008 (2002), [arXiv:astro-ph/0206155](#).
- [64] M. Shiraishi, S. Yokoyama, K. Ichiki, and K. Takahashi, Analytic formulae of the CMB bispectra generated from non-Gaussianity in the tensor and vector perturbations, *Phys. Rev. D* **82**, 103505 (2010), [arXiv:1003.2096 \[astro-ph.CO\]](#).